Int J Earth Sci (Geol Rundsch) (2017) 106:2319–2342
DOI 10.1007/s00531-016-1428-7

ORIGINAL PAPER

Carboniferous rifted arcs leading to an archipelago of multiple arcs in the Beishan–Tianshan orogenic collages (NW China)

Zhonghua Tian[1] · Wenjiao Xiao[2,3,4] · Brian F. Windley[5] · Ji'en Zhang[2] · Zhiyong Zhang[2] · Dongfang Song[2]

Received: 16 June 2016 / Accepted: 18 November 2016 / Published online: 3 December 2016

Abstract The Beishan and East Tianshan Orogenic Collages in the southernmost Central Asian Orogenic Belt (CAOB) record the final stages of evolution of the Paleo-Asian Ocean. These collages and their constituent arcs have an important significance for resolving current controversies regarding their tectonic setting and age, consequent accretionary history of the southern CAOB, and the closure time of the Paleo-Asian Ocean. In this paper, we present our work on the southern Mazongshan arc and the northern Hongyanjing Basin in the Beishan Orogenic Collage (BOC), and our comparison with the Bogda arc and associated basins in the East Tianshan Orogenic Collage. Field relationships indicate that the Pochengshan fault defines the boundary between the arc and basin in the BOC. Volcanic rocks including basalts and rhyolites in the Mazongshan arc have bimodal calc-alkaline characteristics, an enrichment in large ion lithophile elements such as Rb, Ba, and Pb and depletion in high field-strength elements (e.g., Nb and Ta), which were probably developed in a subduction-related tectonic setting. We suggest that these bimodal calc-alkaline volcanic rocks formed in rifted arcs instead of post-orogenic rifts with mantle plume inputs. By making detailed geochemical comparisons between the Mazongshan arc and the Bogda arc to the west, we further propose that they are similar and both formed in arc rifts, and helped generate a Carboniferous archipelago of multiple arcs in the southern Paleo-Asian Ocean. These data and ideas enable us to postulate a new model for the tectonic evolution of the southern CAOB.

Keywords Mazongshan arc · Carboniferous · Subduction-related arc · Beishan · Eastern Tianshan · Central Asian Orogenic Belt

Introduction

The Central Asian Orogenic Belt (CAOB) (Carroll et al. 1995; Buslov et al. 2001; Jahn 2004; Windley et al. 2007; Xiao et al. 2009) or Altaids (Sengör et al. 1993; Wilhem et al. 2012) formed by accretion of island arcs, oceanic islands, ophiolites, accretionary wedges, and microcontinents from the Proterozoic to Mesozoic. The CAOB is located between the Tarim and North China Cratons to the south, and the Siberian and Eastern European Cratons to the north (Fig. 1a). This huge accretionary orogen, which is one of the largest on Earth, was a result of consumption and closure of the Paleo-Asian Ocean (Sengör et al. 1993; Sengör and Natal'In 1996), which gave rise to three major orogenic collage systems, which further consist of several independent orogenic collages (Xiao et al. 2015). The

Electronic supplementary material The online version of this article (doi:10.1007/s00531-016-1428-7) contains supplementary material, which is available to authorized users.

✉ Wenjiao Xiao
wj-xiao@mail.iggcas.ac.cn

[1] Institute of Geology, Chinese Academy of Geological Sciences, Beijing 100037, China

[2] State Key Laboratory of Lithospheric Evolution, Institute of Geology and Geophysics, Chinese Academy of Sciences, Beijing 100029, China

[3] Xinjiang Research Center for Mineral Resources, Xinjiang Institute of Ecology and Geography, Chinese Academy of Sciences, Ürümqi 830011, China

[4] CAS Center for Excellence in Tibetan Plateau Earth Sciences, Beijing 100029, China

[5] Department of Geology, The University of Leicester, Leicester LE1 7RH, UK

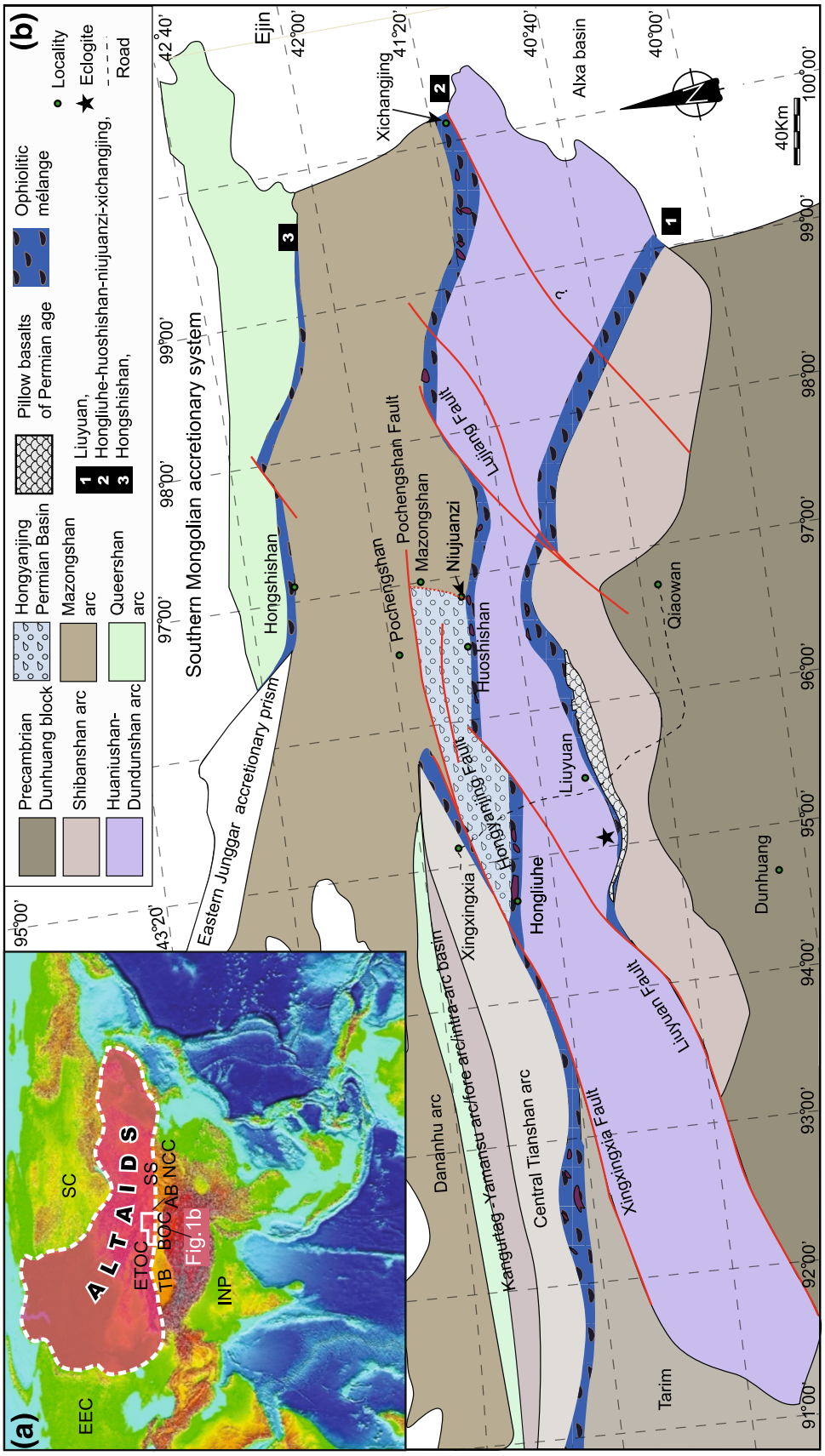

Fig. 1 **a** General tectonic map showing the three collage systems of the CAOB, bound on the north by the Siberian (SC) and Eastern Europe cratons (EEC), and on the south by the Tarim Basin (TB) and North China cratons (NCC) (modified after Sengör et al. 1993; Xiao et al. 2010, 2015). *ETOC* Chinese eastern Tianshan Orogenic Collage, *AB* Alxa Basin, *SS* Solonker suture, *INP* India Plate. **b** Simplified tectonic map of the East Tianshan Orogenic Collage and the Beishan Orogenic Collage (BOC) (modified after Zuo et al. 1990a; Xiao et al. 2004, 2010; Guo et al. 2012; Mao et al. 2012)

Beishan Orogenic Collage (BOC) is located in the southernmost CAOB, and the East Tianshan Orogenic Collage to the west and the Alxa Basin (Xiao et al. 2003) to the east, both of which were formed in the later stage of evolution of the Paleo-Asian Ocean (Xiao et al. 2010) (Fig. 1a). The formation of the BOC and East Tianshan Orogenic Collage records the final attachment of the Tarim craton and associated blocks to the southern accretionary orogenic collages of the southern CAOB (Xiao et al. 2010, 2015). Therefore, both the BOC and East Tianshan Orogenic Collage are of key importance for studying final evolution of the Paleo-Asian Ocean, which is one of the hotly debated issues regarding the accretionary orogenesis, continental growth, and termination of the CAOB.

Two main opinions have been advocated in previous studies: (1) the PAO closed before the Devonian, and the BOC underwent intraplate deformation after the Devonian, after which the whole area underwent rifting in the Carboniferous to Permian (Zuo et al. 1990b; He et al. 2002; Gong et al. 2003; Wang et al. 2010a; Chen et al. 2011; Shu et al. 2011; Su et al. 2011); (2) the Paleo-Asian Ocean in the BOC was closed at the end-Permian (Ao et al. 2012; Guo et al. 2012), and terminal orogenesis was in the Early Triassic (Allen et al. 1994; Xiao et al. 2010; Mao et al. 2014; Tian et al. 2014, 2016). One reason for this controversy is that there are still many rocks and terranes that have not been well mapped, analyzed, understood, and interpreted. This creates and leaves many unanswered questions such as (1) How many terranes and suture zones are there between the Dunhuang block and the Southern Mongolia accretionary system (Fig. 1b)? What are the structure, composition, and tectonic setting of each terrane and mélange that formed at different times? (2) Can these terranes and mélange zones compare with East Tianshan Orogenic Collage to the west and the Alxa (Alashan) block to the east? (3) Which suture zone, of several, is the terminal suture of the Paleo-Asian Ocean in the southernmost Altaids?

In this paper, we present the results of detailed field mapping in the central BOC (southern margin of the Mazongshan arc and northern margin of the Hongyanjing Basin), and of our examination of the petrological, geochemical, and geochronological characteristics of rocks from the Mazongshan arc. Combined with regional studies, these field and laboratory data allow us to discuss and help resolve some of the following questions: (1) What is the composition, tectonic setting, and age of the Mazongshan arc? (2) Were the rocks in the Mazongshan arc the source and provenance for the Hongyanjing Basin to the south? Combined with regional geological data and previous studies, we will compare the Mazongshan arc with the Dananhu–Bogda arc in the East Tianshan Orogenic Collage to the west and discuss the timing of the final suture zone of the Paleo-Asian Ocean, and finally we will provide a new evolutionary tectonic model for the southernmost CAOB near the Beishan.

Geological setting

Tectonic units of the BOC

The BOC connects the Tianshan range to the west and Alxa desert to the east. It tectonically bound by the Tarim–Dunhuang Craton to the south and the southern Mongolian accretionary system to the north, thus occupies a key area in the accretionary CAOB (Fig. 1) (Xiao et al. 2010).

There are several arcs and mélange zones between the Dunhuang block and the Mongolia accretionary system in the BOC (Gong et al. 2003; Zuo et al. 1990a). From south to north, there are the following arcs: the Shibanshan, Shuangyingshan–Huaniushan, Mazongshan, Heiyingshan–Hanshan, and Queershan, and the following ophiolitic mélanges: Liuyuan, Hongliuhe–Xichangjing, Xingxingxia–Shibanjing, and Hongshishan (Ao et al. 2012; Xiao et al. 2010; Mao et al. 2012). Based on our most recent mapping (Tian et al. 2014, 2016), in this paper we simplify the tectonic units from south to north as follows: the Shibanshan arc, the Liuyuan mélange, the Huaniushan–Dundunshan arc (Shuangyingshan–Huaniushan unit or arc in Xiao et al. 2010), the Huoshishan–Niujuanzi ophiolitic mélange (the same belt as Hongliuhe–Xichangjing mélange in Xiao et al. 2010), the Hongyanjing Basin, the Mazhongshan arc (amalgamation of the Heiyingshan–Hanshan unit and the Mazongshan unit in Xiao et al. 2010), the Hongshishan ophiolitic mélange, and the Queershan arc (Fig. 1b). These are described below.

The Shibanshan arc is a continental arc (Guo et al. 2012), situated on the northern margin of the Dunhuang block (Fig. 1b), mainly contains Carboniferous clastic sediments, and Permian volcanic pyroclastic assemblages (Zuo et al. 1990b). North of the Shibanshan arc, the Dundunshan–Huaniushan arc consists of Silurian schists, intrusive rocks and Devonian sediments, basalts, andesites, and rhyolites, and Carboniferous–Permian sediments in the southern part of the arc (Xiao et al. 2010; Zuo et al. 1990a). The volcanic rocks have U–Pb ages of 368.8 ± 3.1 and 370.9 ± 1.3 Ma (Guo et al. 2014). Sandstones at Heishankou on the northern margin of the Shibanshan arc are characterized by lower Ni–Co–Cr–V and slightly higher Th and La contents than those at Liuyuan on the southern margin of the Dundunshan–Huaniushan arc (Guo et al. 2012). Tectonic setting discrimination plots suggest that the Liuyuan sandstones were deposited as detritus from an oceanic island arc, whereas the Heishankou sediments were from an Andean continental margin (Guo et al. 2012). Geochemical data suggest that mafic–ultramafic intrusions

in the Dundunshan–Huaniushan arc are subduction-related, and their emplacement is dated as ~360 Ma by both zircon ID-TIMS U–Pb and SHRIMP U–Pb (Xie et al. 2012).

The Hongyanjing Basin is recognized as an inter-arc basin (Tian et al. 2015), defined by the Pochengshan fault (a branch fault of the Xingxingxia fault) and the Hongyanjing strike-slip fault between the Dundunshan–Huaniushan arc to the south and the Mazongshan arc to the north (Fig. 1b). Sediments in the basin belong to the Lower Zhesi and Upper Hongyanjing Groups, which were strongly deformed during the processes of accretion and collision (Zhang and Cunningham 2012). North of the Hongyanjing Basin, the Mazongshan arc is composed of pyroclastic rocks, diorites, volcanic breccias, andesites, and rhyolites (Zheng et al. 1996) that are undated. Farther north, the Queershan arc in the northernmost Beishan is mainly composed of Silurian to Carboniferous andesites, dacites, and rhyolites, intercalated with grawackes, shales, and slates (Wang et al. 2004).

Lithologies and structures

North of the Pochengshan fault to the west of the Pochengshan village (Fig. 2), the Carboniferous Baishan Group (GBGMR 1969) comprises predominantly igneous rocks, and minor marble and conglomerates. South of the Pochengshan fault (Fig. 2) are Precambrian (GBGMR 1969) marbles and quartzites with minor phyllites and meta-sandstones, and sandwiched between the Precambrian rocks are Cambrian and Ordovician, cherts, shales, and limestones. In the northern Hongyanjing Basin (Fig. 2), the Triassic Shanhujing Group consists of coarse sandstones, siltstones, and shales faulted against the Permian Lower Zhesi and Upper Hongyanjing Groups (GBGMR 1969, 2001).

Between the Cambrian and Permian, the BOC was affected by multiple stages of subduction and collision of arcs and basins giving rise to complex structures (Xiao, et al. 2010) such as thrusted imbricate fans and duplexes, strike-slip faults, and superimposed folds. For example, a giant superimposed fold interference pattern in the Hongyanjing Basin involved fossiliferous Permian sandstones and siltstones, which constrain the age of the terminal Solonker suture (Zhang and Cunningham 2012; Tian et al. 2014, 2015). Besides the Jurassic Pochengshan thrust sheets (Zheng et al. 1996), the important Xingxingxia fault is probably a branch of the Triassic Altyn Tagh fault system extending from the northern margin of the Tibetan plateau (Wang et al. 2010b).

Field mapping

Our mapping at a scale of 1:100,000 was confined to the central BOC (Figs. 1, 2) from the northern margin of the Hongyanjing Basin to the southern margin of the Mazongshan arc. The 90 m digital elevation model (DEM) data were used for constructing the topographic map, and the mapping result is shown in Fig. 3. Some rock types we recognized in the field follow the 1:200,000 geological map (GBGMR 1969). A cross section was drawn perpendicular to the average strike of the structures and bedding of sedimentary rocks (Fig. 3). The area has an arid climate and low, well-exposed hills (Fig. 4a).

Geological characteristics of the Mazongshan arc

On the southern side of the Mazongshan arc (northern part of Fig. 3), the Baishan Group intruded by granodiorites (Fig. 4b) consists of conglomerates, volcanic rocks, and marbles (Fig. 3). Cross-section C–D (Fig. 4c) shows detailed rock composition and stratigraphic–structural relationships of the Baishan Group. From southwest to northeast (Fig. 4c), a thick layer (~200 m) of rhyolites erupted and covered the Baishan conglomerates (Fig. 4c, d). The Baishan conglomerates contain marble pebbles (3 mm–50 cm diameter) in a marble matrix (Fig. 5a). Boulders in conglomerates contain Early Carboniferous fossils such as *Syringopora* sp., *Kueichouphyllum* sp., and *Gigantoproductus* sp. (GBGMR 1969), which indicate that the depositional age was younger than Early Carboniferous. Some of the strongly deformed clasts (Fig. 5a) in conglomerates may have been affected by the Pochengshan fault (Fig. 3). Toward northeast of the cross section (Fig. 4c), tuff and pyroclastic rocks erupted and covered the rhyolites. These rocks (including conglomerate, rhyolite, tuff, and pyroclastic rocks) are connected with another suite of rocks including mudstones, rhyolites, tuff, and pyroclastic rocks by a reverse fault, which indicate a stratigraphic repetition. Further northeast, another reverse fault (high-angle dipping to NE) was recognized between pyroclastic rocks (footwall) and conglomerate (hanging wall). Northeast of the conglomerates, ~300 m thick rhyolites erupted and covered the conglomerate. Then, a strike-slip fault separates the marbles and pyroclastic rocks into two units in the middle of the cross section (Fig. 4c). North of the pyroclastic rocks, tuffs and pyroclastic rocks erupted and covered the deformed marbles. A syncline is easily observed in the marble according to the opposite dip directions of S_1 foliations in the two limbs. The deformed marbles were covered by the pyroclastic rocks in fault contacts with another suite of pyroclastic rocks (~800 m). At last (Fig. 4c), a granodiorite intruded the pyroclastic rocks (Fig. 4b, c), indicating that the eruption age of volcanic rocks was younger than the granodiorites.

Most of the rocks in the Carboniferous Baishan Group are not metamorphosed, and only a few of them experienced very low-degree metamorphism (greenschist facies).

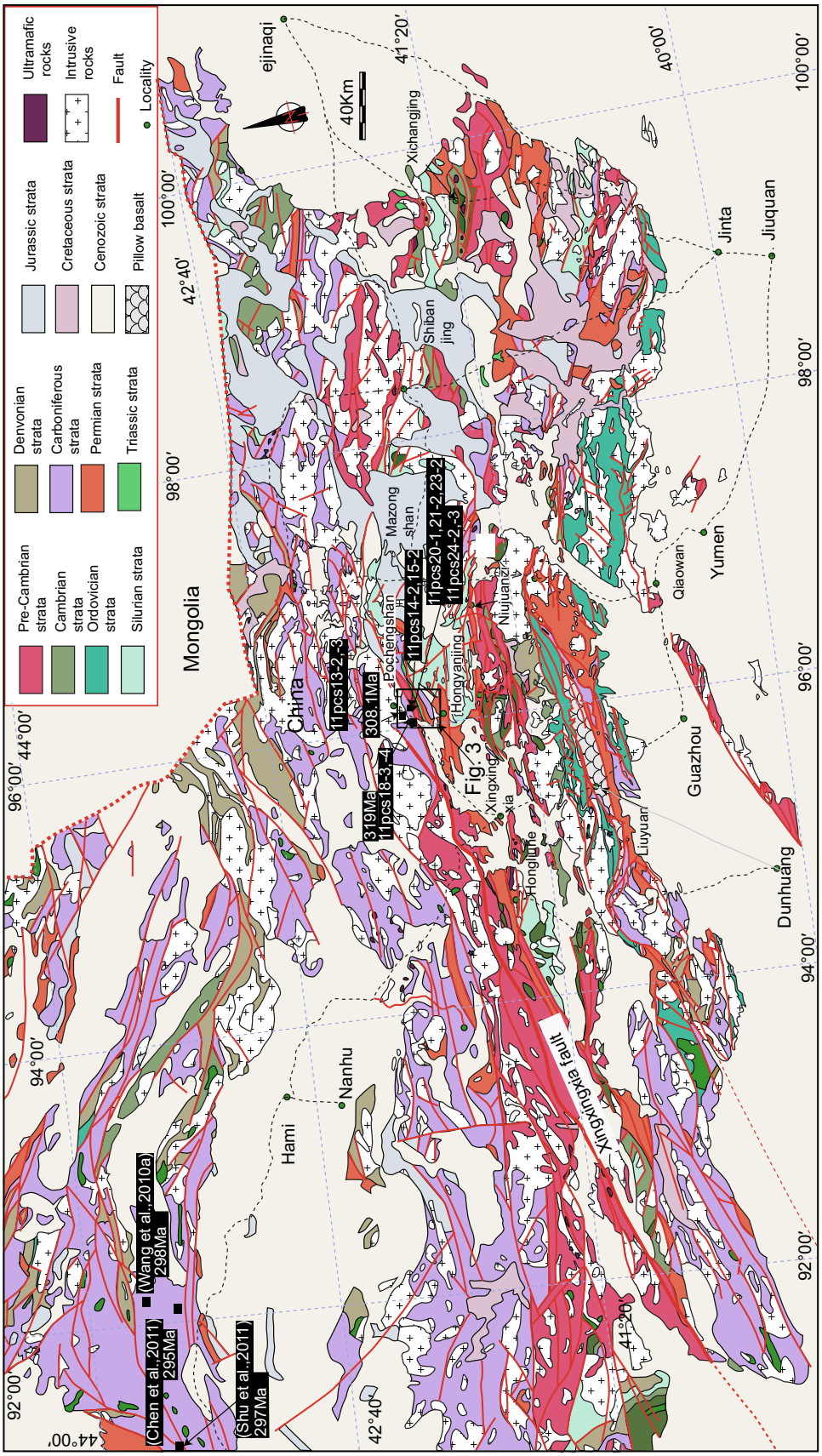

Fig. 2 Geological map of the Beishan Orogenic Collage including Xinjiang and Gansu Beishan in the southernmost part of Altaids (Modified after 1,000,000 geological maps). The area of Fig. 3 is marked. Sample locations in this study and some previous studies are marked

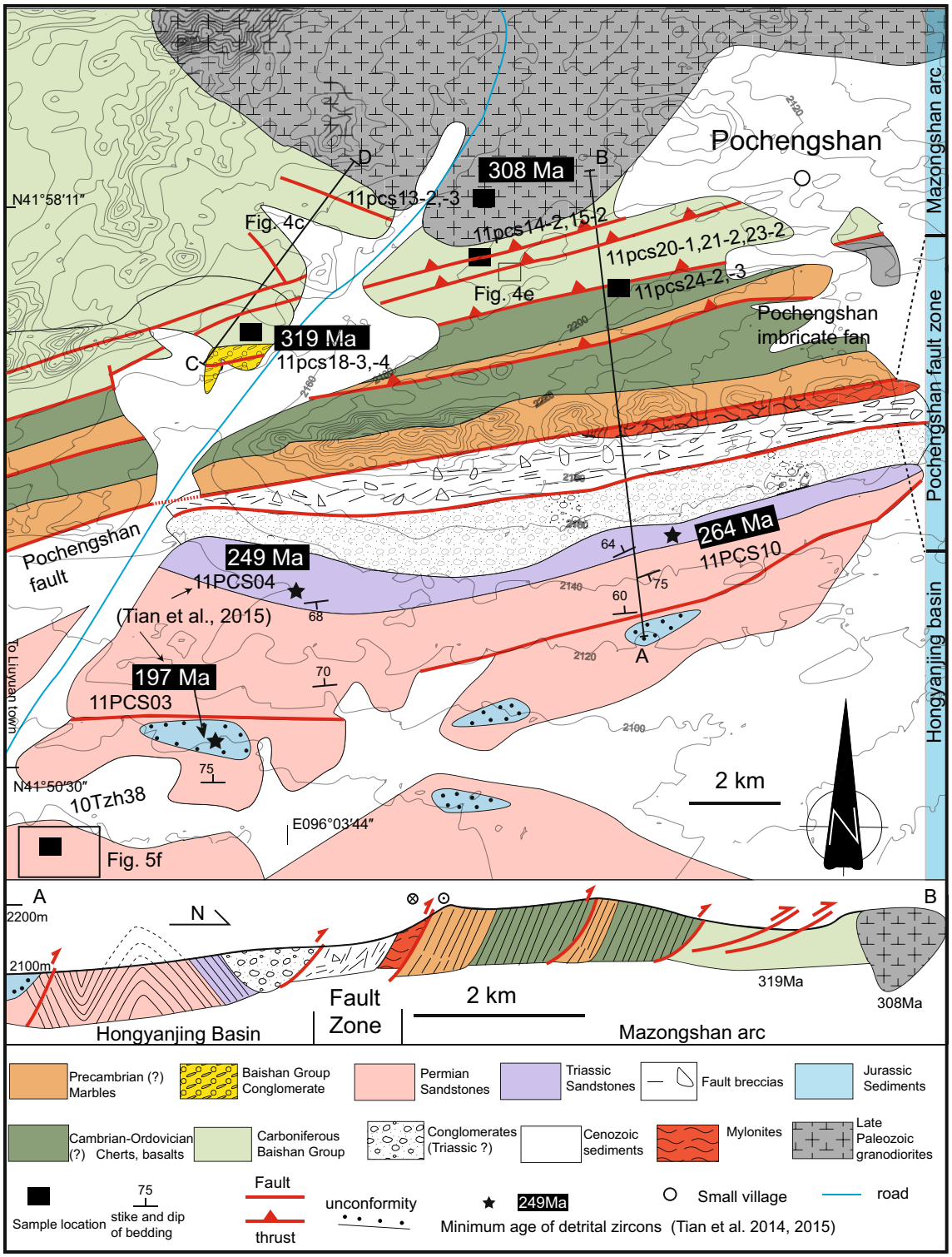

Fig. 3 Field geological map showing the southern Mazongshan arc and northern margin of the Hongyanjing Basin. Geologic mapping was based on our field observations, and the arc basin boundary was based on a Google Earth satellite image. In addition, 90 m digital elevation model (DEM) data were used for making the topographic map. The area of Figs. 4e and 5f is marked. The cross-section C–D of Fig. 4c is also marked

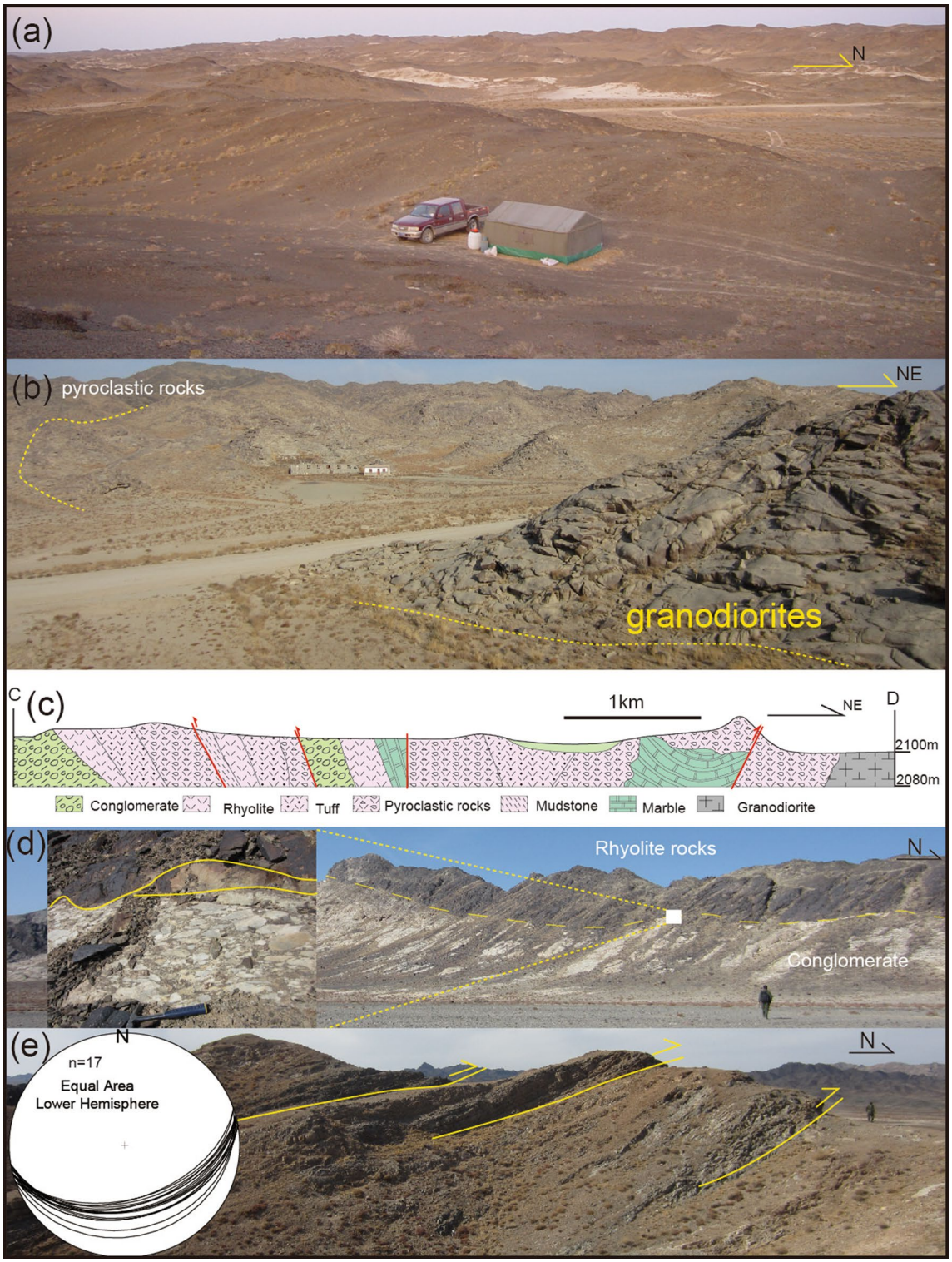

Fig. 4 Photographs showing **a** landforms in the map area which is arid Gobi Desert; **b** field features of granodiorites in the southern margin of the Mazongshan arc; this granodiorite intruded Carboniferous pyroclastic rhyolite; **c** cross-section C–D shows the detail stratigraphic–structural relationships of the Carboniferous Baishan Group; **d** the conformable (*dashed line*) relationship between the Carboniferous pyroclastic rhyolite and conglomerates in the Baishan Group. **e** Thrusts in the Carboniferous Baishan Group; fault planes dip nearly due south (~165°) at 20°–50° (*inset* stereographic projection)

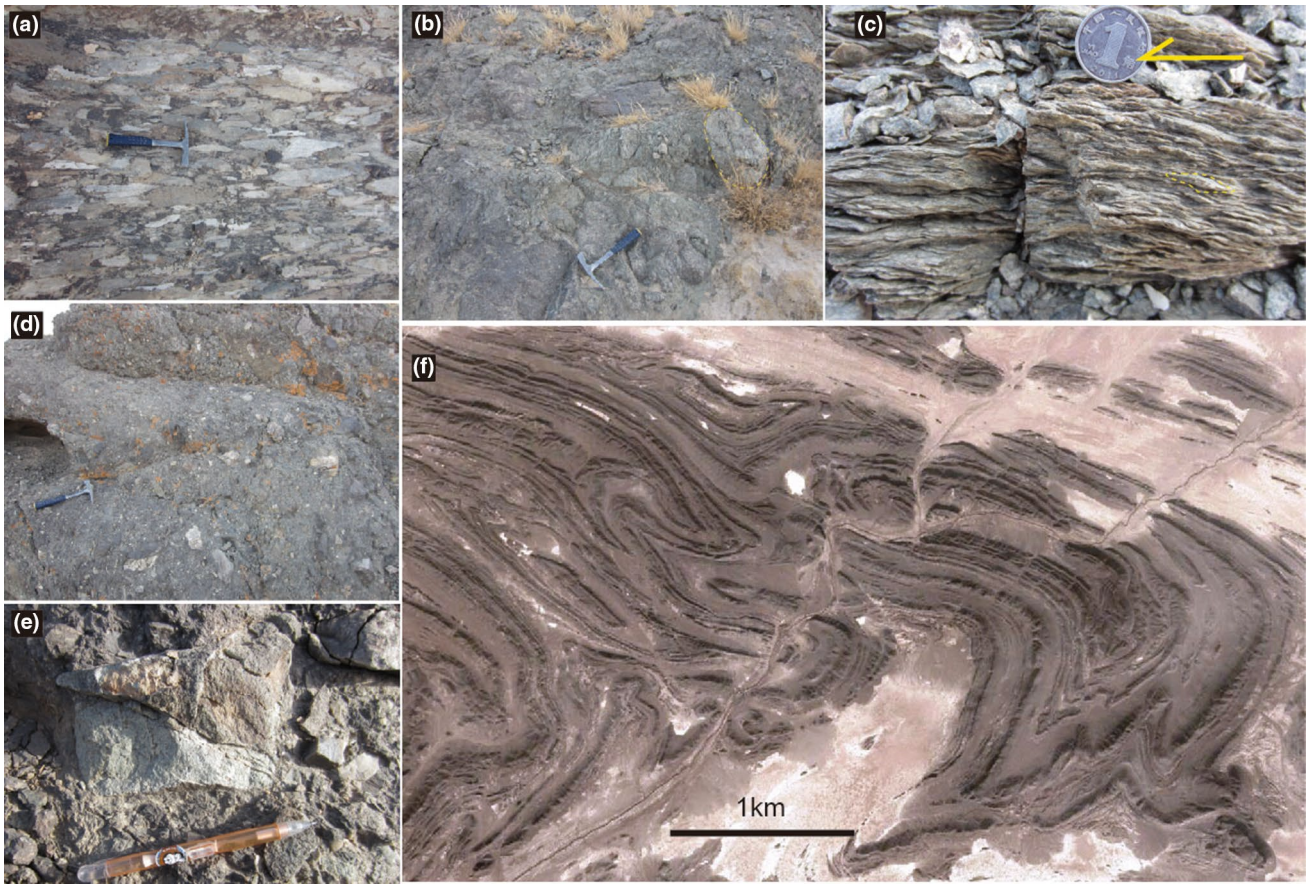

Fig. 5 Photographs showing **a** conglomerate in the Baishan Group, the matrix of which is marble, and the deformed pebbles are also marble and have diameters of 3 mm–50 cm; **b** mylonites crushed by the Pochengshan fault zone; **c** S–C fabric in the mylonites indicates sinistral movement; **d**, **e** the conglomerates in a conglomerate belt in the northern margin of the Hongyanjing Basin; **f** strongly deformed Permian sediments in the Hongyanjing Basin

About one kilometer east of the cross-section C–D, the Baishan Group was affected by many thrusts (Figs. 3, 4e), which dip almost to the south (~165°) with dip angles of 20°–50°. The Baishan Group is connected with the Cambrian–Ordovician strata (No credible isotopic and fossil evidence) by a thrust fault. At the boundary of these rock units, many volcanic rocks including felsic rhyolites and mafic basalts crop out. South of the Carboniferous Baishan Group, Cambrian and Ordovician rocks are sandwiched between Precambrian rocks (Fig. 3). We mapped in detail the Precambrian (No credible isotopic and fossil evidence) marbles and Cambrian–Ordovician cherts and basalts (both undated), which contain imbricate fans.

Pochengshan fault

To the west of the Pochengshan fault (Fig. 1), the Xingxingxia fault has a complicated history and structure (Hendrix et al. 2001; Webb and Johnson 2006; Xu et al. 2008). It is 0.3–2 km wide and at least 600 km long, and has evidence of dextral strike-slip in the Late Paleozoic–Early Mesozoic (Xiao et al. 2010), and sinistral movement at ~240–235 Ma (Wang et al. 2010b). The Pochengshan fault zone, which is a branch of the Xingxingxia transcurrent fault (or shear zone) (Wang et al. 2010b), separates the Mazongshan arc to the north and the Hongyanjing Basin to the south (Fig. 3). The Pochengshan fault is located between the Pochengshan imbricate fans to the north and Triassic conglomerates and sandstones to the south (Fig. 3). This fault contains mylonites that were crushed by strike-slip shears (Fig. 5b), which have S–C sinistral kinematic indicators similar to the Xingxingxia fault (see also Wang et al. (2010b). S–C fabric developed in the schists (Fig. 5c) experienced greenschist facies metamorphism with the metamorphic mineral assemblage of muscovite + chlorite + albite + quartz. Feldspar experienced ductile deformation forming δ porphyroclast surrounded by mica, chlorite, and quartz, which indicate sinistral kinematic movements (Fig. 5c). South of the mylonite zone, the Pochengshan fault has brittle structures with fault breccias.

Hongyanjing Basin

South of the Pochengshan fault zone and faulted against the Hongyanjing Basin, there is a wide belt (~1 km) of conglomerates (Fig. 5d, e) that have poorly sorted, angular, and immature boulders, which indicate short transportation and rapid deposition. The age of these conglomerates is unknown; they must be younger than Early Triassic because they conformably overlie Triassic sandstones. The conglomerate belt is not shown on previous geological maps.

Beneath the conglomerate belt, yellow sandstones and siltstones were marked as Triassic on the 1: 250,000 geological map (GBGMR 2001), but as Permian on the 1:200,000 geological map (GBGMR 1969). Tian et al. (2015) demonstrated that the youngest detrital population of zircons from the sandstones has an age of 249.2 Ma; this Early Triassic age postdates the formation age of the sandstones. South of these Triassic sandstones, dark sandstones and siltstones were subdivided into the Zhesi Group and the Hongyanjing Group on the 1:200,000 geological map (GBGMR 1969). The 1390-m-thick Zhesi Group consists of siltstones, bioclastic limestones, shales, and conglomerates, and the ~4.3-km-thick Hongyanjing Group is composed of shales, siltstones, sandstones, and conglomerates. These sediments that were deposited under marine to terrigeneous conditions contain rich fauna and flora including *Glottophyllum cuneatum, Callipteris* cf. *zeilleri, C.* cf. *invancevia, Iniipteris sibirica,* and *Nellipteris* (GBGMR 1969). The *Glottophyllum cuneatum* in the Hongyanjing Group is a typical Late Permian Angara flora (Boersma and Broekmeyer 1987). Most of the sedimentary rocks are not metamorphosed; only a few of them experienced very low-degree metamorphism (greenschist facies).

A magnificent, large-scale fold interference pattern is well exposed in weakly metamorphosed sediments of the Zhesi and Hongyanjing Groups in the Hongyanjing Basin (Fig. 5f). Recently, Zhang and Cunningham (2012) and Tian et al. (2013) provided detailed descriptions and interpretations of these superimposed folds. Undeformed coarse sandstones and conglomerates, which rest unconformably on the refolded Permian–Early Triassic rocks, are marked as the Jurassic Shuixigou Group on the 1: 250,000 geological map (GBGMR 2001); this age is confirmed by the youngest age of 197.9 Ma of detrital zircons from the sandstones (Tian et al. 2015).

Petrochemistry

In order to investigate the tectonic setting of the Mazongshan arc, 11 representative samples of intrusive and eruptive rocks were crushed for major and trace element analysis to provide information on the element distributions and petrogenesis. The samples are divisible into two groups, the intrusive rocks of 11pcs13-2, 11pcs13-3, and 11pcs14-2, and the extrusive rocks of 11pcs15-2, 11pcs18-3, 11pcs18-4, 11pcs20-1, 11pcs21-2, 11pcs23-2, 11pcs24-2, and 11pcs24-3. The major and trace element compositions of those samples are shown in -T 1. Sample locations are marked in Fig. 3, and detailed experimental methods are given in "Major and trace elements" section of Appendix.

Petrography

Of the many available thin sections from the Mazongshan arc and Hongyanjing Basin, nine representative ones are described here. 10Tzh38 is a sandstone sample collected from the Hongyanjing Basin, sample 11pcs13 is an intrusive rock, and the others (11pcs15, 11pcs18, 11pcs20, 11pcs21, 11pcs22, 11pcs23, and 11pcs24) are volcanic rocks sampled from the south margin of the Mazongshan arc (Fig. 3), the microscopic characteristics of which are shown in Fig. 6.

11pcs13 is a Late Carboniferous granodiorite (its precise age will be constrained in "Geochronological data" section) that is mainly composed of quartz, plagioclase, and amphibole (Fig. 6a). Similar to the volcanic rocks, the granodiorites also have a large area of exposure (>100 km^2, Figs. 2, 3) cropping out in the south margin of the Mazongshan arc. Field relationships show that the granodiorite intruded the volcanic rocks (Fig. 4b, c). Samples 11pcs15, 11pcs18, and 11pcs20 are lithic tuffs, mainly composed of pyroclastic mineral grains of quartz, K-feldspar, plagioclase, which range in diameters from 0.1 to 2 mm (Fig. 6b–d), together with lithic fragments (such as volcanic lithic grains with felsic texture (Lvf) in Fig. 6d). The precise age of sample 11pcs18 is given in "Geochronological data" section.

More detail microscope features are shown for sample 11pcs21 in Fig. 6e, and many relatively large plagioclase grains (~1.5 mm width) were surrounded by rhyolitic matrix, which locally retains its pyroclastic flow structure. Unlike plagioclase grains in sample 11pcs21, sample 11pcs22 mainly consists of quartz grains ranging in diameter from 0.1 to 0.5 mm, and a uniform pyroclastic matrix (Fig. 6f). Thin section for sample 11pcs23 (Fig. 6g) predominantly focuses on two kinds of mineral grains, i.e., plagioclase and quartz. These two minerals are also surrounded by pyroclastic matrix similar to 11pcs21 and 11pcs22. Sample 11pcs24 consists of plagioclase and altered pyroxene, and opal minerals fill the spaces between the plagioclases (Fig. 6h). Different from those felsic volcanic rocks described above (Samples 11pcs15, 11pcs18, 11pcs20, 11pcs21, 11pcs22, and 11pcs23), sample 11pcs24 has obvious mafic volcanic rock features.

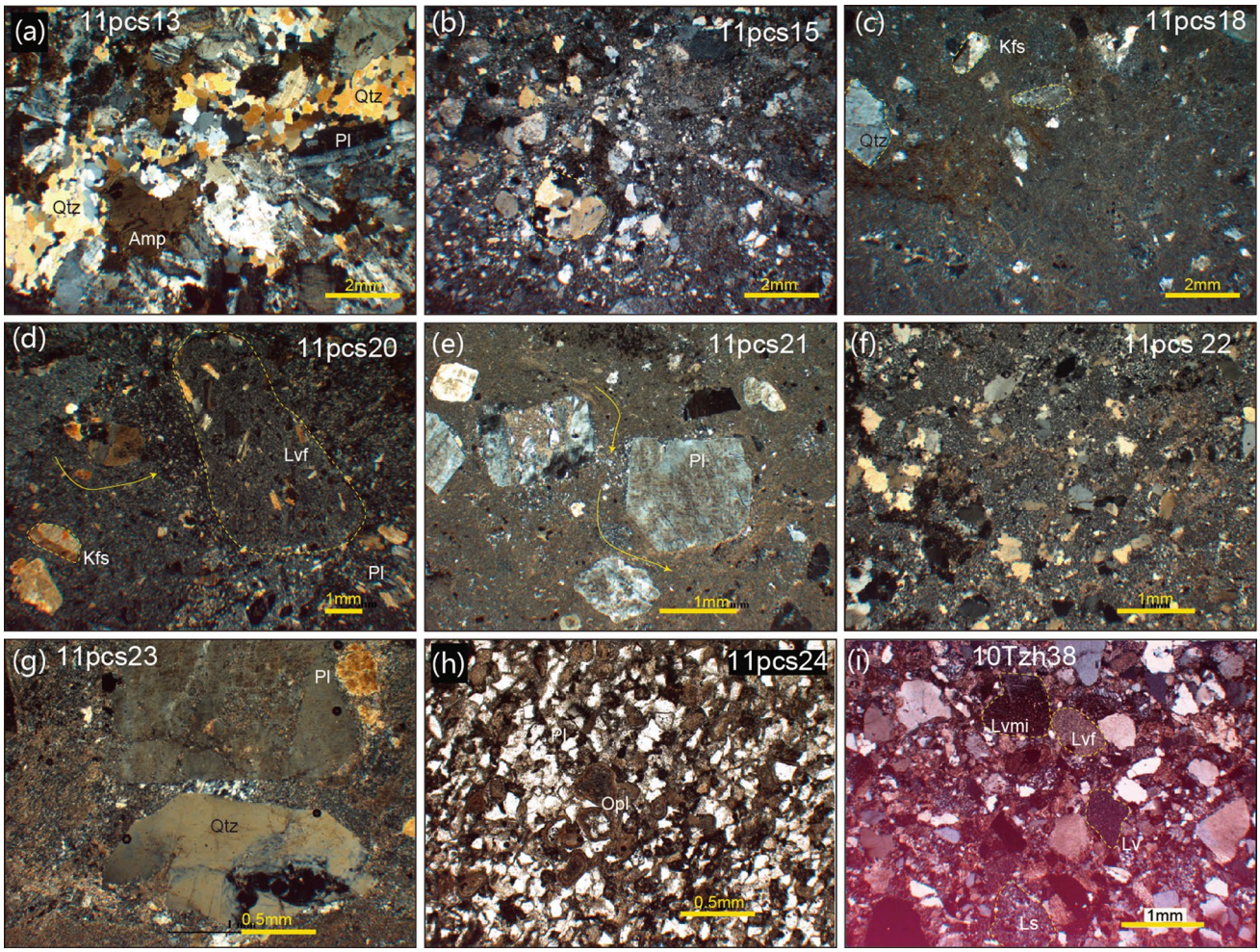

Fig. 6 Photomicrographs (cross-polarized light) of samples 11pcs13 (**a**), 11pcs15 (**b**), 11pcs18 (**c**), 11pcs20 (**d**), 11pcs21 (**e**), 11pcs22 (**f**), 11pcs23 (**g**), and 11pcs24 (**h**) of igneous rocks on the southern margin of the Mazongshan arc. Locations of these samples are shown in Fig. 3. 11pcs13 (**a**) mainly composed of quartz, plagioclases, and amphiboles. 11pcs15 (**b**), 11pcs18 (**c**), 11pcs20 (**d**), 11pcs21 (**e**), 11pcs22 (**f**), and 11pcs23 (**g**) mainly composed of pyroclastic grains and tuffaceous matrix. The pyroclastic grains consist of quartz, K-feldspar, and plagioclase; the lithic tuff has a felsic composition. Rhyolitic flow structure is well developed in 11pcs21 and indicated with a *curved arrow* (**e**). 11pcs24 (**h**) consists of plagioclase and altered pyroxenes indicating a mafic volcanic rock feature. Lvf in (**c**): volcanic lithic grain with felsic texture. 13Tzh 38 (**i**) is a sandstone sample from the Hongyanjing Basin; it consists of not only single-component mineral grains but also multi-component lithic fragments such as Lv, Lvmi, Lvf, and Ls. Lvmi, volcanic lithic grain with microlithic texture; Lv, volcanic lithic grains; Ls, sedimentary lithic grain

13Tzh 38 is from the Hongyanjing Group (Fig. 3). This group is mainly composed of siltstones and sandstones in the Hongyanjing Basin south of the Mazongshan arc. Sandstones in the basin are fine- to coarse-grained, poorly sorted and contain angular grains of very low sphericity (Tian et al. 2013), which indicate a very close clastic material transportation. The framework minerals of sample 10Tzh 38 are mainly quartz, plagioclase, feldspar, and some lithic fragments. Lithic fragments consist of predominantly volcanic lithic grains (Lv) including volcanic lithic with microlithic texture (Lvmi) and volcanic lithic with felsic texture (Lvf) (Fig. 6i). Moreover, sedimentary lithic grain (Ls) can also be observed in the thin section (Fig. 6i). The lithic fragments observed in sandstones of the Hongyanjing Basin could be come from the volcanic rocks cropping out in the Mazongshan volcanic arc. Most of the mineral grains and lithic fragments are not metamorphosed.

In general, thin sections from the south margin of the Mazongshan arc are mainly composed of pyroclastic mineral grains of quartz, K-feldspar, plagioclase surrounding by pyroclastic matrix. Most of the volcanic rocks show felsic feature except for sample 11pcs24 displaying mafic feature (e.g., 11pcs24). Volcanic clastic material observed in the thin section of sample 10Tzh 38 from the Hongyanjing Basin indicates a very close provenance, which further

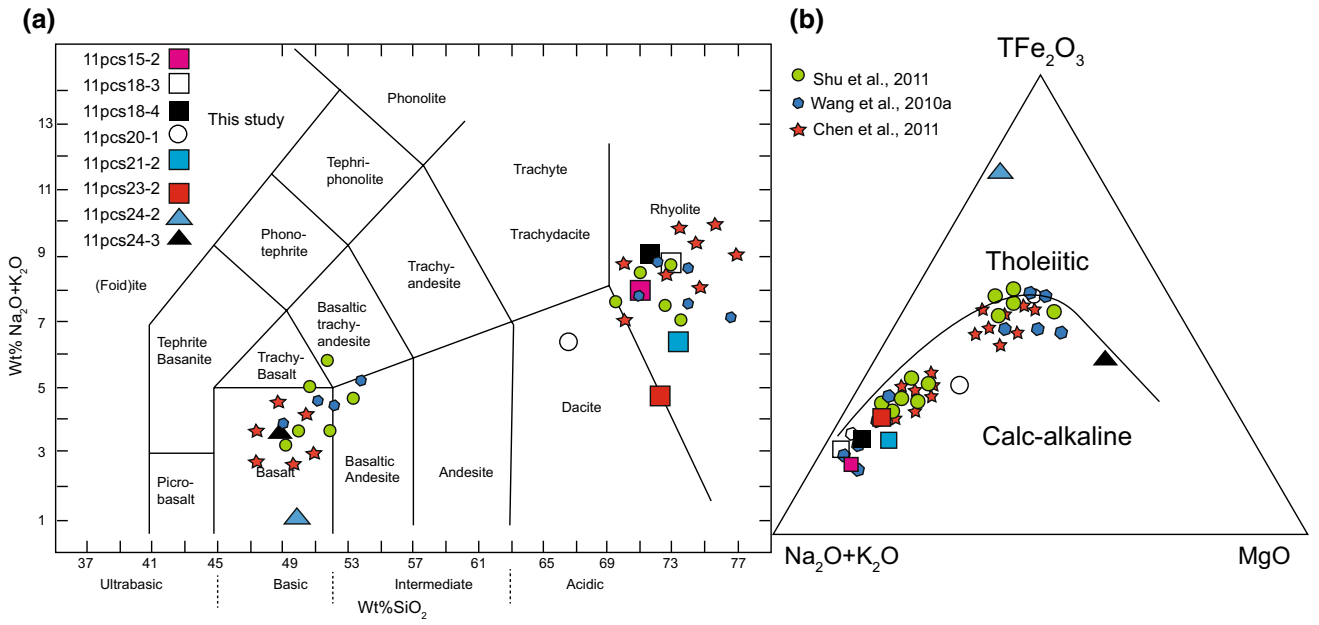

Fig. 7 Petrochemical diagrams of volcanic rocks from the Mazongshan arc. **a** SiO_2 versus K_2O (after Peceerillo and Taylor 1976); **b** (Na_2O + K_2O)–FeO^T–MgO (Pearce 1996). *Red star* denotes data from Chen et al. (2011); *purple hexagon* data from Wang et al. (2010a), and *green circle* data from Shu et al. (2011); the others are all from this study

imply the Mazongshan volcanic arc was the major source region for the Hongyanjing Basin.

Geochemistry

Major elements

Representative samples from the Mazongshan arc can be divided by their SiO_2 contents into two groups: (1) Felsic rocks with a range from 77.29 to 67.51%, and (2) Mafic rocks with a range from 52.65 to 50.41% (Supplementary Table 1). The extrusive rocks show variable high loss on ignition (LOI) (0.56-6.35%), especially samples 11pcs24-2 (6.35%) and 11pcs24-3 (6.08%), indicating different degrees of alteration (Supplementary Table 1). The rhyolitic (felsic) samples have SiO_2 contents that range from 71.49 to 76.28%, and relatively high Al contents (from 14.03 to 14.85%) except for sample 11pcs23-2 (only 10.45%). Two basalt samples have SiO_2 contents that range from 50.41 to 52.65%. Sample 11pcs24-2 has an extremely low Al content (2.11%) compared with sample 11pcs24-3 (14.54%). The Ca contents of these two samples are 28.15% for 11pcs24-2 and 8.21% for 11pcs24-3, respectively.

The major element compositions were normalized to 100% (water-free) before plotting on the discrimination diagrams. In the SiO_2 versus Na_2O + K_2O diagram (Fig. 7a), five samples plot in the rhyolite field, two in the basalt field, and only one in the dacite region. In the AFM diagram (Fig. 7b), all the samples classify as calc-alkaline, except for 11pcs24-2, which plots in the tholeiitic field. These geochemical distributions are indicative of bimodal calc-alkaline volcanic rocks, which most likely formed in a tectonic rift (Chen et al. 2011).

Trace and rare earth elements

The trace and rare earth elements of eight samples including two granodiorites (11pcs13-2, 11pcs13-3), one granitoid (11pcs14-2), four pyroclastic rocks (11pcs15-2, 11pcs18-3, 11pcs20-1, and 11pcs21-2), and one basalt (11pcs24-2) were plotted on primitive-mantle (PM)-normalized multi-element diagrams (Fig. 8a, c) and chondrite-normalized REE pattern diagrams (Fig. 8b, d). Firstly, the primitive-mantle-normalized (pm) (Sun and McDonough 1989) element patterns of samples (11pcs13-2, 11pcs13-3, 11pcs14-2, and 11pcs14-2) are enriched in large ion lithophile elements (LILE) such as Rb and Pb. Considering the crustal levels, on the chondrite-normalized REE pattern diagrams (Fig. 7b), the LREEs are more enriched than the HREE. Secondly, compared with OIB, the primitive-mantle-normalized (pm) (Sun and McDonough 1989) element patterns of these samples are strongly depleted in high field-strength elements (HFSE) (e.g., Nb and Ta) and enriched in large ion lithophile elements (LILE) such as Rb, Ba, and Pb (Fig. 7c). On the chondrite-normalized REE pattern diagrams (Fig. 7d), the LREEs are enriched compared with the HREE, and the fractionated trends of

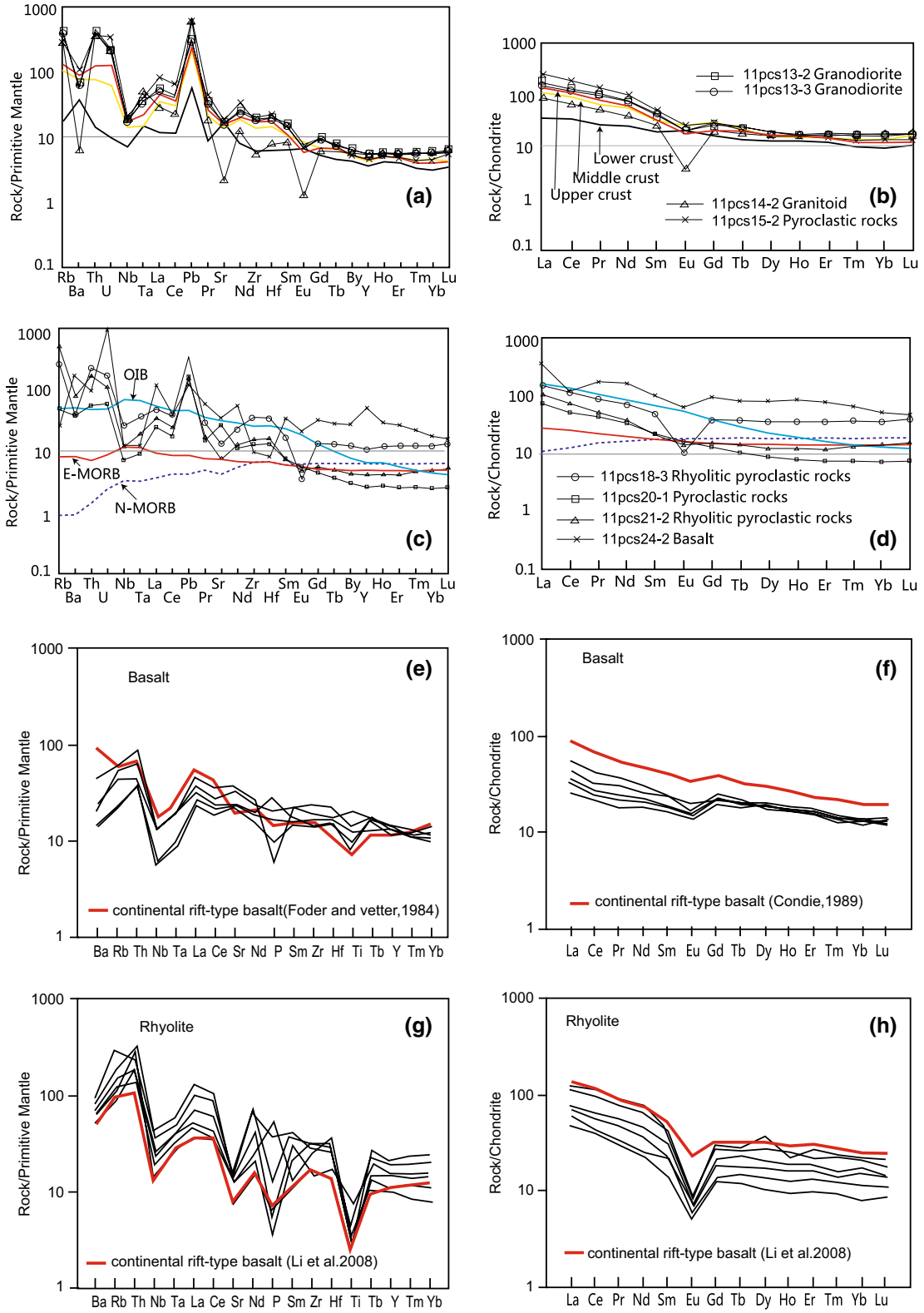

Fig. 8 Primitive-mantle (PM)-normalized multi-element diagrams (**a**, **c**) and chondrite-normalized REE patterns (**b**, **d**) for granodiorites and volcanic rocks from the Mazongshan arc. **e**–**g** are modified after Chen et al. (2011), which show the geochemical characteristic of basalts and rhyolites sampled from the Bogda arc in the TOB. The chondrite, PM, N-MORB, E-MORB, and OIB values are from Sun and McDonough (1989). The average values of the upper, middle, and lower crusts are from Rudnick and Gao (2003). *N-MORB* normal mid-ocean ridge basalts, *E-MORB* enriched mid-ocean ridge basalts, *OIB* oceanic island basalts

the samples are between those of OIB and E-MORB or N-MORB, except for sample 11pcs24-2.

Geochronological data

Sample 11pcs18, a pyroclastic rhyolite, is from the southern Mazongshan arc (Fig. 3). Figure 9 shows typical zircon CL images of 25 grains about 60–100 μm in size from this sample. Most have long columnar morphologies, and a few, such as grains 4 and 19, are conchoidal. According to their zoning structures, they can be divided into two groups: the first lacks core–rim structures and is homogeneous, indicating rapid cooling during crystallization (e.g., from felsic volcanic rocks); the second group contains only four grains (grain 9, 16, 17, and 20) shows oscillatory zoning.

Isotopic ages and data are shown in Supplementary Table 2. $^{206}Pb/^{238}U$ ages range from 309 Ma to 334.5 Ma, and concentrate in a small area close to or on the Concordia line (Fig. 10a). The $^{206}Pb/^{238}U$ weighted average age is 319.6 ± 3.4 Ma (MSWD = 1.3) (Fig. 10b). We interpret this Early Carboniferous age as the time of eruption of the pyroclastic rhyolite.

Figure 9 also shows 25 zircons from sample 11pcs13, which all have long columnar morphologies. Oscillatory zoning is well developed, indicating slow cooling during crystallization. Isotopic ages and data are shown in Supplementary Table 3. $^{206}Pb/^{238}U$ ages range from 290.7 Ma to 320.5 Ma, and concentrate in a small area close to or on the Concordia line (Fig. 10c). The $^{206}Pb/^{238}U$ weighted average age is 308.1 ± 3.8 Ma (MSWD = 3.1) (Fig. 10d); we interpret this Late Carboniferous age as the time of intrusion of the granodiorite. Sample locations are marked in Fig. 3, and detailed experimental methods are given in "Zircon cathodoluminescence and geochronology" section of Appendix.

Discussion

The geological map (Fig. 3), and petrochemical and geochronology data for the intrusive and extrusive rocks from the Mazongshan arc and the Hongyanjing Basin enable us to discuss the tectonic setting and age of formation of the Mazongshan arc. By integrating with previous regional geological data, we can provide new geochronological evidence for the provenance of the Hongyanjing Basin, and then we will discuss the age and tectonic setting of the Mazongshan arc. More importantly, we will compare the Mazongshan arc with the Dananhu–Bogda arc, because this is along strike to the west in the East Tianshan Orogenic Collage. Finally, we will present a new model for the tectonic evolution of the BOC and East Tianshan Orogenic Collage, and discuss its implications for the late evolution of the CAOB.

Provenance for the Hongyanjing Basin

The Hongyanjing Basin was most likely an inter-arc basin between the Mazongshan arc and the Huaniushan–Dundunshan arc (Fig. 1) (Tian et al. 2015). In order to investigate the provenance of sediments in the basin, Tian et al. (2015) studied U–Pb detrital zircon ages of sandstones from the Hongyanjing Basin, and concluded that most sediments were derived from an Early Silurian (peak age of 442 Ma) source and a Late Carboniferous to Early Permian (peak age of 305–298 Ma) source. After comparing with the detrital zircon distributions and characteristics of nearby arcs and terrenes, Tian et al. (2015) concluded that the major source of sediments in the Hongyanjing Basin was most likely the Huaniushan–Dundunshan arc to the south and the Mazongshan arc to the north, plus some contributions from the Central Tianshan arc to the west. Firstly, the south Huaniushan–Dundunshan arc was a likely provenance region for the Hongyanjing Basin, because (1) the Huoshishan–Niujuanzi ophiolitic mélange belt contains many Silurian to Devonian blocks with crystallization ages ranging from 444 to 410 Ma (Tian et al. 2014), and it is located in the northern part of Huaniushan–Dundunshan arc south of the Hongyanjing Basin (Fig. 1b); (2) southeast of the Hongyanjing Basin, meta-sediments in the Caohulehade area on the northern margin of the Huaniushan–Dundunshan arc have an age spectrum with a prominent age peak at 442 Ma, which is exactly the same as that of the Hongyanjing Basin (Song et al. 2013). Secondly, detrital zircon data from Central Tianshan meta-sediments have a peak age of 444 Ma (close to 442 Ma), which indicates a likely provenance (Ma et al. 2012).

However, there is no evidence that the Mazongshan arc, which is located to the north of Hongyanjing Basin, was a source region for the basin. So, the question arises: Where did the Late Carboniferous to Early Permian (peak age of 305–298 Ma) zircons in the Hongyanjing Basin come from. Fortunately, our new well-dated granodiorite (11pcs13 with an age of 308.1 ± 3.8 Ma) and pyroclasitic rhyolite (11pcs18 with an age of 319.6 ± 3.4 Ma) come the southern margin of the Mazongshan arc, providing evidence that this arc was the Late Carboniferous to Early Permian (peak age of 305–298 Ma) sedimentary provenance for the Hongyanjing Basin. In addition, volcanic clastic fragments observed in the sample of 10Tzh 38 from the Hongyanjing Basin indicate that the Mazongshan volcanic arc was the major source region for this basin. Accordingly, the data in this paper suggest that the major source of sediments in the Hongyanjing Basin was most likely the Mazongshan arc to the north, as well as the Huaniushan–Dundunshan arc to

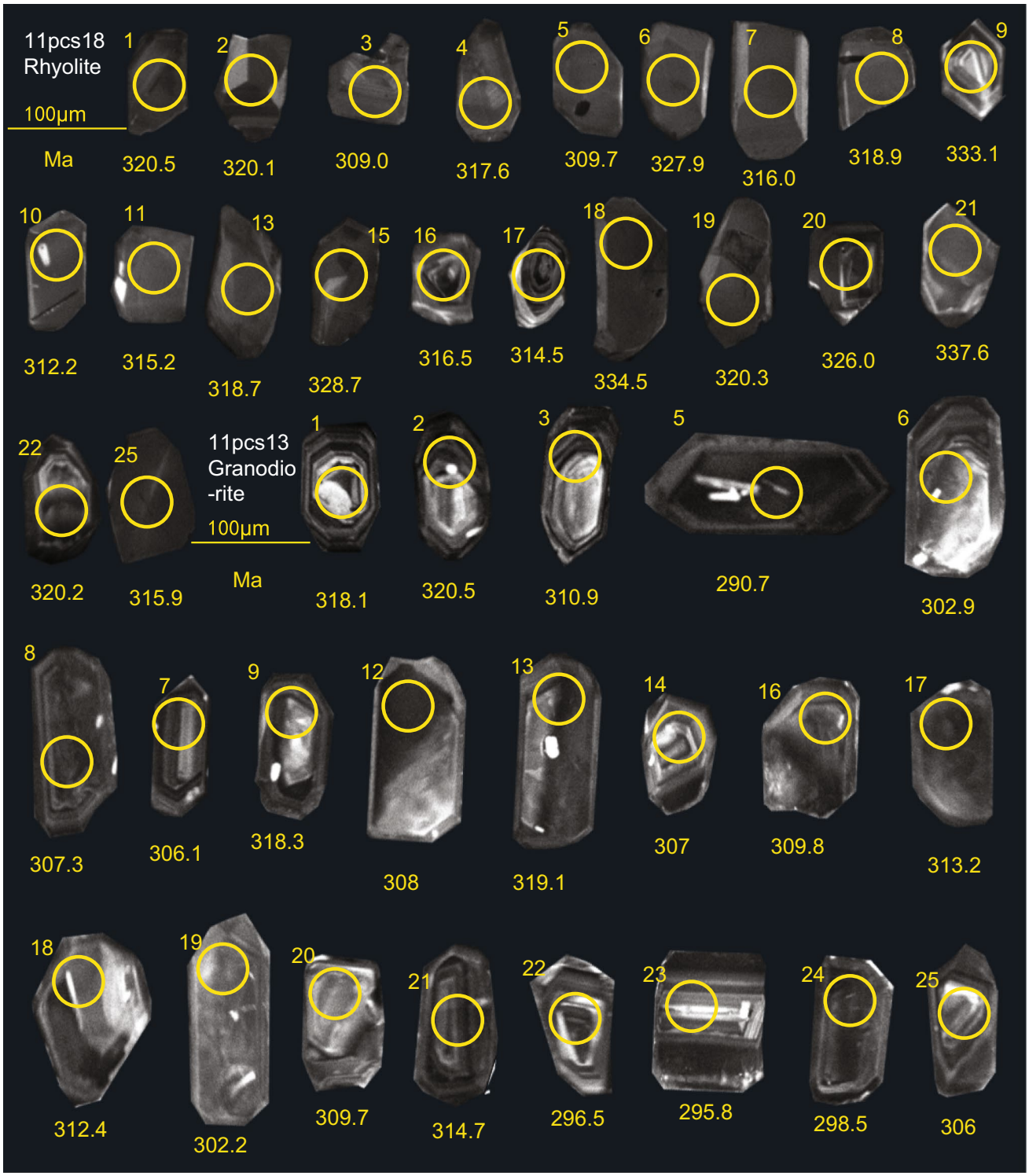

Fig. 9 Cathodoluminescence (CL) images of zircons from samples 11pcs18 and 11pcs13, on which analytical spots with a diameter of 32 μm are marked (*yellow circles*). CL images were made with a SX51 Electron Probe Microanalyzer for high-resolution and spectroscopy at the IGGCAS in Beijing

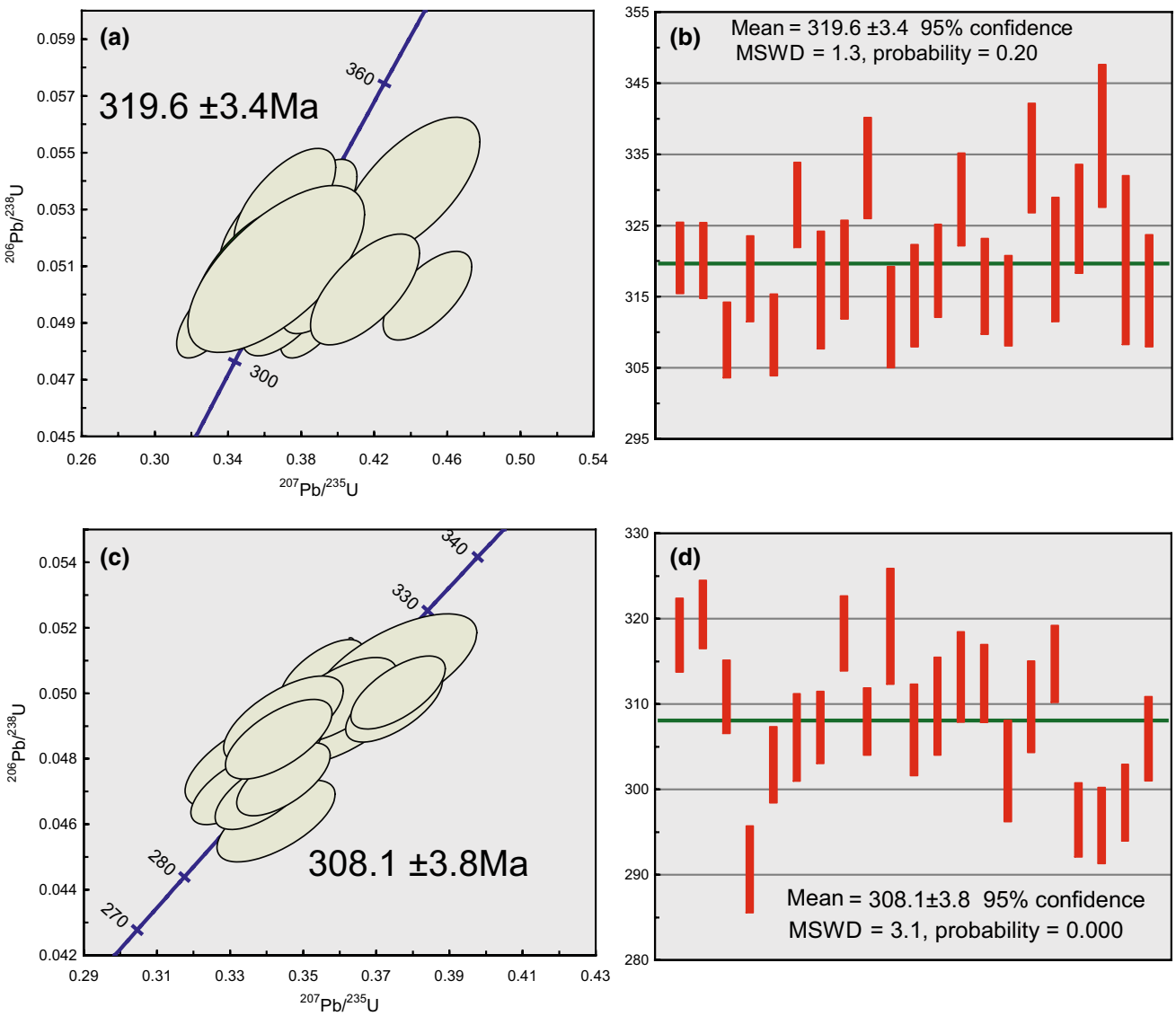

Fig. 10 **a**, **c** U–Pb Concordia age diagrams for zircons from pyroclastic rhyolite 11pcs18 and granodiorite 11pcs13 in the Mazongshan arc. Data-point error ellipses are 1σ; **b**, **d** showing the weighted average ^{238}U–^{206}Pb ages, respectively. All the data are listed in Supplementary Tables 2 and 3

the south, and to a lesser extent the Central Tianshan arc to the west.

Age and tectonic setting of the Mazongshan arc

Many accretionary orogenic belts worldwide underwent complicated tectonic process such as subduction, accretion, and collision with associated deformation and metamorphism (Cawood et al. 2009). It is particularly difficult to unravel the ages and tectonic settings of allochthonous fragments in mélanges and as accreted oceanic island arcs, continental margin arcs, fore-arc/inter-arc/back-arc basins, and ophiolites. Isotopic dating and geochemical analysis of magmatic and sedimentary rocks provide some means to define the age, tectonic setting, and accreted framework of an orogenic belt. The CAOB contains many such problems of accretion, including the BOC in which we are here unravelling the ages of arcs, the along-strike correlations of arcs, and the provenance of sediments from eroded arcs to basins.

Age of the Mazongshan arc

Zuo et al. (1990b, 1991) recognized that the eastern part of the Mazongshan arc (southeast of the Pochengshan fault, Fig. 1) consisted of weakly metamorphosed, Late Paleozoic volcanic rocks including felsic extrusives, and Zuo et al. (1990b) reported older rocks such as metamorphosed

Mid–Late Ordovician felsic volcanic rocks and clastic sedimentary rocks. Geochemical data indicate that the volcanic rocks have a calc-alkaline signature (Liu and Wang 1995), but their age was still unknown. The western Mazongshan arc (northwest of the Pochengshan fault Fig. 1) consists of high-grade metamorphic gneisses, schists, and migmatites, as well as low-grade metamorphic rocks that contain microfossils of Cambrian to Silurian age (Zuo et al. 1991; Liu and Wang 1995; Dai and Gong 2000; Du et al. 2003), and overlying Permian sandstones, tuffaceous conglomerates, and purple mudstones (Zuo et al. 1990b). But the precise ages of the arc and sediments are still unknown. For this study, we carried out U–Pb zircon dating of igneous rocks that are the main components of the Mazongshan arc (Fig. 2). An intrusive granodiorite was dated as Carboniferous with an age of 308.1 ± 3.8 Ma, and a volcanic rock was dated as Late Carboniferous with an age of 319.6 ± 3.4 Ma.

We should note that Xiao et al. (2010) and Mao et al. (2012) considered that the Mazongshan arc and the Heiyingshan–Hanshan arc (Fig. 3 in Xiao et al. 2010, and Fig. 1b in Mao et al. 2012, north of the Mazongshan arc) were different arcs. The Heiyingshan arc contains Carboniferous felsic volcanic rocks, and carbonate and clastic sedimentary rocks including terrestrial clastic rocks that are intercalated with cherts, limestones, and volcanic rocks (Zuo et al. 1990b). Geochemical data show that the volcanic rocks have a calc-alkaline, subduction-related signature (Liu and Wang 1995; Wei et al. 2004; Huang and Jin 2006). In common with the Heiyingshan arc, the Hanshan arc unit (Fig. 3 in Xiao et al. 2010) is characterized by low-pressure, high-temperature metamorphic rocks, and the original rocks were considered to belong to a Paleozoic arc (Liu and Wang 1995) or a Precambrian microcontinent (Zuo et al. 1990b); whole-rock Rb–Sr and/or Sm–Nd model ages have confirmed a Precambrian age (He et al. 2002; Nie et al. 2002). Nie et al. (2002) also reported that the Hanshan arc contains many calc-alkaline granitic intrusions, the isotopic ages of which range from Carboniferous to Triassic (zircon U/Pb and muscovite Ar–Ar dating). Moreover, Ao et al. (2016) concluded that the Hanshan unit is an accretionary prism, which accreted continuously from the Silurian to the Devonian (457–367 Ma) on the northern margin of the Shuangyingshan–Mazhongshan composite arc. Accordingly, there was likely an accretionary prism in the Hanshan arc, which later underwent subduction and accretion, and the Heiyingshan–Hanshan arc and the Mazongshan arc may have amalgamated forming a composite arc in the Carboniferous–Early Permian. In this paper, we therefore suggest that this composite arc is called the Mazongshan arc, which mainly consists of Carboniferous igneous and sedimentary rocks.

Tectonic setting

On the major element discrimination diagram (Fig. 7b), most of the mafic rocks are defined as calc-alkaline, except for one sample that plots in the tholeiitic field. Calc-alkaline volcanic rocks are widespread in and typical of mature oceanic island arcs and active continental margin arcs, except for a few that occur in rifts (Sheth et al. 2002). We consider that the petrochemical features of the calc-alkaline volcanic rocks in the Mazongshan arc are most consistent with generation in an island arc. In addition, basalts erupted in volcanic arcs often show enrichments in Sr, K, Rb, and Ba (and sometimes Th) relative to Ta to Cr (Pearce 1982). Volcanic arc calc-alkaline basalts and shoshonites are usually enriched in alkalis and alkaline earth elements, and the elements of Th, Ce, P, and Sm, and have a low abundance of incompatible element such as Ta, Nb, Zr, Hf, Ti, Y, and Yb (Pearce 1982). Accordingly, our granodiorites and pyroclastic rhyolites have an enrichment in large ion lithophile elements (LILE) such as Rb, Ba, and Pb (except for sample 11pcs14-2), and a depletion in high field-strength elements (HFSE) (e.g., Nb and Ta) (Fig. 8a, c). These geochemical relations are similar to those in volcanic arcs (Pearce. (1982). Our samples also have a slight enrichment in LREE compared with the HREE (Fig. 8b, d). Taken together, all these variables suggest that the granodiorites and pyroclastic rhyolites were generated in an island arc and were contaminated by fluids that were likely mobile in such a supra-subduction zone.

Comparison with the Dananhu–Bogda arc in eastern Tianshan

The East Tianshan Orogenic Collage, located to the west of the BOC, underwent complex subduction and accretion processes in the Late Paleozoic, and it was formed by accretion of many island arcs, ophiolites, oceanic islands, and accretionary wedges (Xiao et al. 2004; Windley et al. 2007). The East Tianshan Orogenic Collage and BOC are roughly separated by the Xingxingxia and the Pochengshan fault (Fig. 11). Tectonically, the East Tianshan Orogenic Collage in NW China is divisible (south to north) into the Central Tianshan arc, the Kanggurtag–Yamansu fore-arc basin, the Dananhu–Bogda arc, the Xiaopu intra-arc basin, and the Harlik arc (Fig. 11) (Xiao et al. 2004).

Petrochemical and age data of igneous rocks from the Mazongshan arc suggest correlation with the Dananhu–Bogda arc in the East Tianshan Orogenic Collage (Fig. 11). Firstly, considering the major element distributions in the AFM diagram (Fig. 7), the geochemical characteristics of rocks in the Mazongshan arc are comparable to those of equivalent rocks from the Bogda arc, most of them plotting

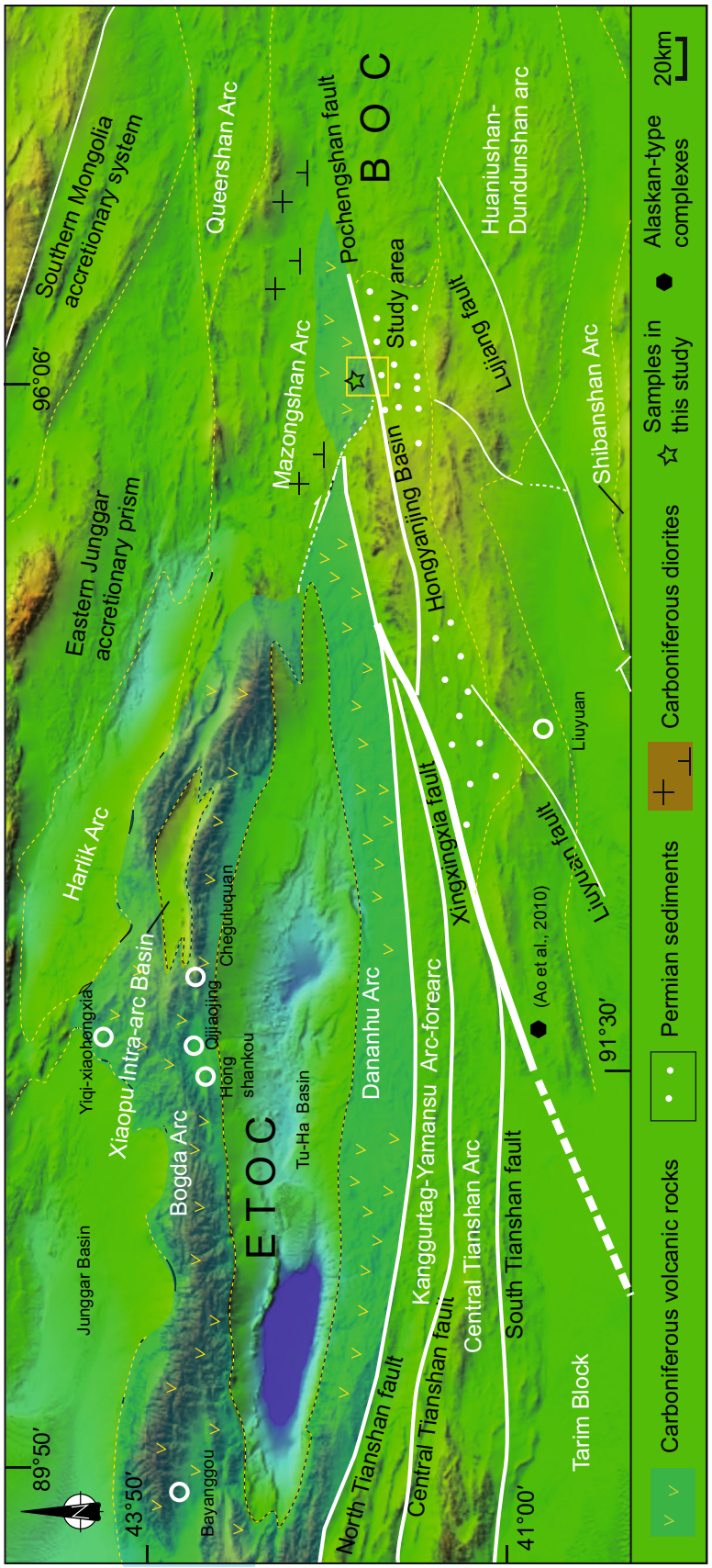

Fig. 11 A digital elevation map of the East Tianshan Orogenic Collage (ETOC) and BOC created by 90 m digital elevation data (DEM) download from the USGS ftp site, provided by the NASA Shuttle Radar Topographic Mission (SRTM). The map also shows the tectonic units in the East Tianshan Orogenic Collage and the Beishan Orogenic Collage (BOC)

in the basalt and rhyolite fields (Fig. 7a). In common with the Bogda arc, rocks in the Mazongshan arc are defined as calc-alkaline and volcanic except for one sample that plots in the tholeiitic field (Fig. 7b). Chen et al. (2011) proposed that these geochemical features indicate a bimodal high-K calc-alkaline affinity, which is characteristic of a rift tectonic setting.

Secondly, on the trace element diagrams, the basalts are characterized by high abundances of Th, U, and Pb and depletions in Nb, Ta, and P (Fig. 8e, f), and the rhyolite samples show an affinity to aluminous A-type granites with enrichments in K + Na, Zr, Ce, and depletions in P, Nb, Ta, and Ti (Chen et al. 2011) (Fig. 8g, h). And all samples (except for 11pcs14-2) have enrichments in large ion lithophile elements (LILE) such as Rb, Ba, and Pb, and depletions in high field-strength elements (HFSE) (e.g., Nb and Ta) (Fig. 8a, c). In addition, the rhyolites in the Baiyanggou area (Fig. 11) are characterized by depletions of Ba, Nb, and Sm, and enrichments in Rb, Th, and Zr, and the basalts by a LERR-enriched pattern and depletions in Ba, Nb, and Zr, and enrichments in Rb, Th, Ti, Ce, and Hf (Shu et al. 2011). In the Yiqi-Xiaohongxia area (Fig. 11), the basalts have high Al (Al_2O_3 = 16.2–16.68%) and are slightly enriched in incompatible elements Ba, Zr, Hf, and LREE, but relatively depleted in Nb–Ta and Th (Wang et al. 2010a). The rhyolites in this area belong to the high-K calc-alkaline series, are relatively rich in trace elements Rb, Th, Zr, Hf, K, and significantly depleted in Ba, Sr, P, Ti, Nb, Ta (Wang et al. 2010a). In all, the rocks (particularly basalts and rhyolites) in the Bogda area are geochemically analogous to those in the Mazongshan arc, which are likewise enriched in large ion lithophile elements (LILE) and depleted in high field-strength elements (HFSE).

Thirdly, LA–ICP–MS dating of zircons from four rhyolites and two basalts in the Bogda arc by Chen et al. (2011) yielded Early Permian ages ranging from 295.8 ± 2.8 to 293.3 ± 1.7 Ma. A porphyritic gabbro has a (SHRIMP) zircon U–Pb age of 288 ± 3 Ma, and a rhyolite a (LA–ICPMS) zircon U–Pb age of 297 ± 2 Ma (Shu et al. 2011), and two rhyolites in the Yiqi-Xiaohongxia area east of the Bogda arc have Rb–Sr ages of 278 ± 2 Ma (1σ) and 296 ± 2 Ma (1σ) (Wang et al. 2010a). And from the Mazongshan arc, we have obtained new ages of 308.1 ± 3.8 Ma for a granodiorite and 319.6 ± 3.4 Ma for a volcanic rock. The above data demonstrate that the magmatic Dananhu–Bogda and Mazongshan arcs were both generated in Late Carboniferous to Permian times.

The petrochemical data and isotopic ages of the Bogda arc by Chen et al. (2011), Shu et al. (2011), and Wang et al. (2010a) are all very close to our results from the Mazongshan arc. However, there are diverse opinions about the tectonic setting of the Bogda arc. For example, Chen et al. (2011) suggested that the bimodal rocks were generated in a post-orogenic continental rift. Shu et al. (2011) also believed that the Baiyanggou olistostrome and accompanying bimodal volcanic rocks were linked to an extensional setting that developed on the south of the present Bogda Shan. Wang et al. (2010a) pointed out that the significant depletion in Nd and Ta, and the enrichment in Rb in the Bogda rhyolites are similar to those of rhyolites in continental rifts, which were generated by melting of lower crust with plagioclase as an important relic mineral in the source. Finally, while studying the bimodal basalts and rhyolites in the Hongshankou area in the Central Tiashan (East Tianshan Orogenic Collage in Fig. 11), Chen et al. (2013) reported that the mafic (~347 Ma) and felsic (~344 Ma) rocks are enriched in light rare earth elements (LREE) and large ion lithophile elements (LILE), and are depleted in high field-strength elements (HFSE), and so proposed that the island arc-type bimodal character reflected back-arc extensional magmatism induced by subduction of the Junggar plate during the Late Paleozoic.

Accordingly, we put forward that these basaltic–rhyolitic rocks were formed in an arc-related tectonic setting, rather than in a post-orogenic rift tectonic setting, for the following reasons: (1) The basalts in the Bogda area have high Al (Wang et al. 2010a, b; Chen et al. 2011), and high Al (>16%) basalts are typical of an arc-related setting; (2) Pearce (1982) demonstrated that volcanic arc calc-alkaline basalts usually have enrichments of alkali and alkaline earth elements and Th, Ce, P, and Sm, and a low abundance of incompatible elements such as Ta, Nb, Zr, Hf, Ti, and Yb. The geochemical data for the volcanic rocks (basalts and rhyolites) in the Bogda arc and the Mazongshan arc are consistent with this conclusion of Pearce (1982). These bimodal rocks are commonly generated in an island arc and contaminated by fluids that are likely present in a supra-subduction zone.

We therefore suggest that the bimodal calc-alkaline volcanic rocks formed in a rifted arc and not in a post-orogenesis rift affected by a mantle plume. Such an arc-related, subduction-related rift setting could be an inter-arc, intra-arc or back-arc basin or rifted margin. Rifted arcs are common in archipelagos, like present-day Indonesia, which typically have several arcs with fore-, intra-, and back-arc basins.

Implications and tectonic evolution

The tectonic settings of the BOC and East Tianshan Orogenic Collage in the Late Carboniferous to Early Permian have long been controversial; post-orogenic extensional rifts (Zuo et al. 1990b; Gong et al. 2003; Xia et al. 2008; Wang et al. 2010a; Chen et al. 2011; Shu et al. 2011; Su et al. 2011) or orogenic subduction/accretion arcs (Xiao et al. 2010; Guo et al. 2012; Tian et al. 2014; Zhou et al.

2016). Our new structural, geochemical, and isotopic age data integrated with much published literature lead to the conclusion that the Mazongshan arc in the central BOC could only have formed in an arc-related, subduction-related tectonic setting, which may have been a rifted arc such as an inter-arc basin. We cannot agree with a post-orogenic rift setting controlled by a mantle plume (Xia et al. 2008; Su et al. 2011).

Many tectonic models have been proposed for the late evolution of the BOC (Zuo et al. 1990b; Gong et al. 2003; Xiao et al. 2010; Tian et al. 2014) and East Tianshan Orogenic Collage (Xiao et al. 2004; Chen et al. 2011; Shu et al. 2011). From our new data in combination with the efficacies of these models, we are now able to present a new model (Fig. 12), which better portrays the timing and tectonic evolution of the main terranes in the Late Paleozoic to earliest Mesozoic in the BOC and East Tianshan Orogenic Collage. The main orogenic process was the accretion of an arc/accretionary prism to a composite arc. Our new tectonic evolutionary model illustrated in Fig. 12 is explicable as follows:

1. In the Early Carboniferous (Fig. 12a), on the northern side of the Liuyuan Ocean (a branch of the Paleo-Asian Ocean), the composite Huaniushan–Dundunshan arc that had formed in the Early Paleozoic (Tian et al. 2014) was accreted to the Mazongshan arc on a northerly dipping subduction zone. On the northern side of the Central Tianshan Ocean, the Dananhu–Harlik composite arc was connected along strike to the Mazongshan arc to the east. On the southern side of the Liuyuan Ocean, southward subduction led to the formation of the Shibanshan arc on the northern margin of the Dunhuang Block (Guo et al. 2012). The Central Tianshan arc formed by north-dipping subduction of the South Tianshan ocean in front of the Tarim block (Xiao et al. 2004, 2015). The Tarim block might have been accreted to the Central Tianshan arc to the north, or may have been accreted to the Dunhuang block to the east (Xiao et al. 2010). This might explain why the Tarim block was bordered by a passive continental margin, while the Dunhuang block was an active continental margin in the Late Paleozoic.
2. In the Late Carboniferous, north of the Liuyuan–Central Tianshan Ocean, the composite Huaniushan–Dundunshan arc was rifted forming the Queershan arc to the north of the Hongshishan inter-arc basin in the BOC, and the Harlik arc to the north of the correlative Xiaopu inter-arc basin in the East Tianshan Orogenic Collage (Xiao et al. 2004). At this stage, bimodal calc-alkaline volcanic rocks formed in both the BOC and East Tianshan Orogenic Collage, which were in arc-related, subduction-related rift tectonic settings. In addition, the Huaniushan–Dundunshan arc accreted to the Mazongshan arc, forming the Huoshishan–Niujuanzi ophiolitic mélange—Fig. 12b (Tian et al. 2014).
3. In the Early Permian (Fig. 12c), the Hongshishan inter-arc ocean in the BOC and the Xiaopu inter-arc ocean in the East Tianshan Orogenic Collage closed, forming the Hongshishan ophiolitic mélange. At this stage, because of the north-dipping subduction of the Liuyuan Ocean plate, in the BOC the Hongyanjing inter-arc basin formed between the Huaniushan–Dundunshan arc and the Mazongshan (Tian et al. 2015). Similarly, the Tu-Ha Basin formed between the Dananhu arc and the Bogda arc to the west. The Central Tianshan arc might have got accreted to the Dananhu arc forming an ophiolitic mélange zone. In addition, the Tarim and Dunhuang blocks began to be mutually amalgamated, forming a huge accretionary wedge between them. Early Permian Alaskan-type mafic–ultramafic complexes formed by subduction of a middle ocean ridge on the northern part of the Shibanshan arc (Ao et al. 2010; Xiao et al. 2010).
4. In the End-Permian to Early Triassic, in the BOC area the Liuyuan Ocean closed, forming the Liuyuan ophiolitic mélange (Fig. 12d), while the Kumishi Ocean (or south Tianshan Ocean) closed in the East Tianshan Orogenic Collage forming the Kumishi ophiolite. The final suture zone is cryptic, the position of which is below the toe of the pre-collisional accretionary complex after the closure of the intervening ocean (Xiao et al. 2013). The first-order tectonic boundary is the cryptic suture that separates the upper plate sequences (accretionary complex, fore-arc and arc) from the lower plate sequences (passive margin and basement of the craton) (Xiao et al. 2013). It was this cryptic suture that recorded the termination of the consumed South Tianshan Ocean in the East Tianshan Orogenic Collage and Liuyuan Ocean in the BOC (Fig. 12d). In previous studies, the ophiolitic mélanges and backstop arcs were commonly interpreted misleadingly as the major suture zones.

All the arcs, basins, ophiolitic mélanges, and accretionary wedges mutually amalgamated to form the East Tianshan Orogenic Collage and BOC in the southern CAOB. The first episode of exhumation in the northern Tarim, occurring in the Mid-Permian to Triassic, is here suggested to be induced by docking of the Tarim Craton and final amalgamation of the CAOB (Zhang et al. 2016). In the Mid-Mesozoic, intense intra-continental deformation took place in the BOC (Zheng et al. 1996; Zhang and Cunningham 2012), in South Mongolia (Johnson et al. 2001; Lamb et al. 2008) and on the China–Mongolia boundary (Davis et al. 2001). This intraplate deformation produced a number of major overthrusts with displacements of over

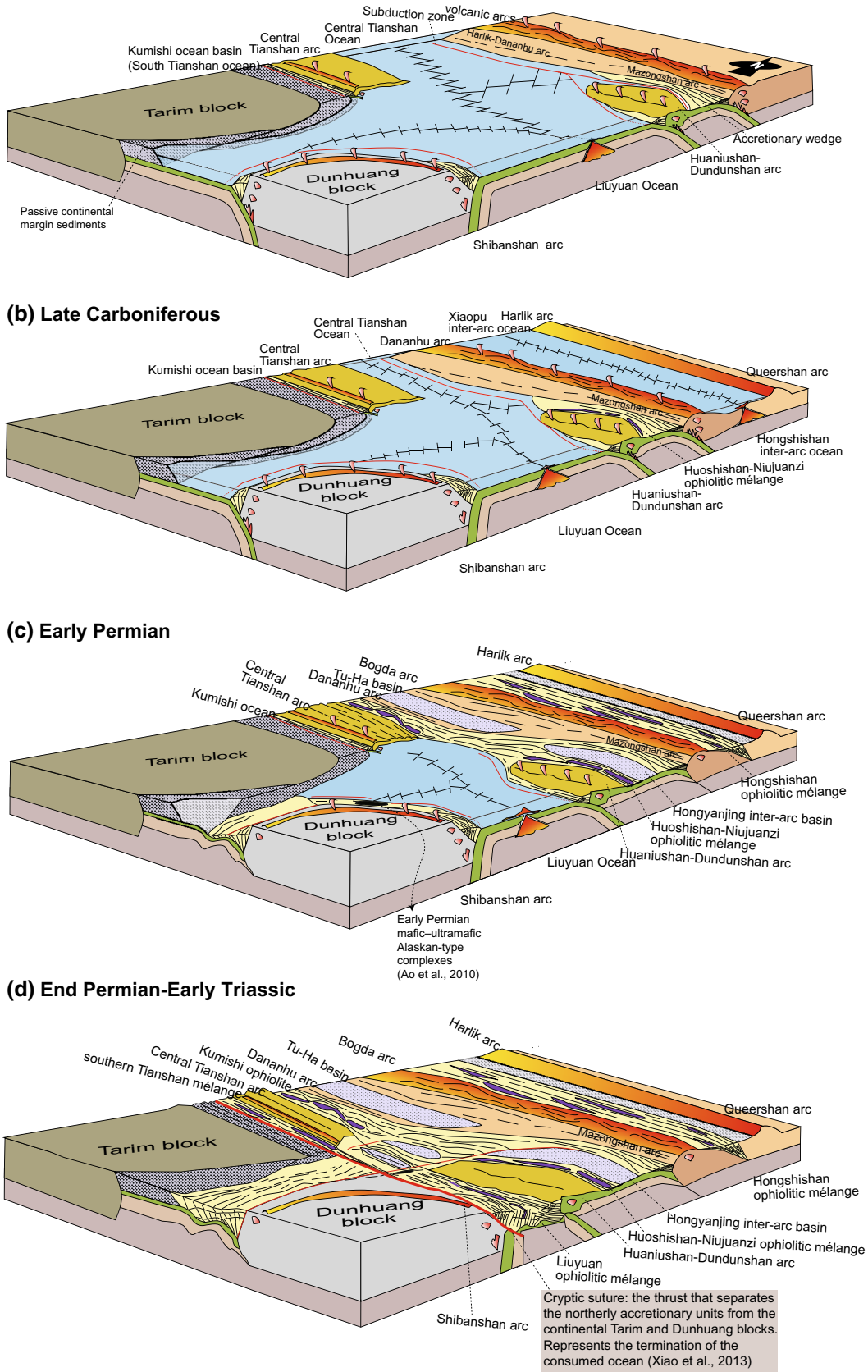
(a) Early Carboniferous
Subduction zone
volcanic arcs
Central Tianshan Ocean
Central Tianshan arc
Kumishi ocean basin (South Tianshan ocean)
Harlik-Dananhu arc
Mazongshan arc
Tarim block
Accretionary wedge
Huaniushan-Dundunshan arc
Dunhuang block
Liuyuan Ocean
Passive continental margin sediments
Shibanshan arc
(b) Late Carboniferous
Central Tianshan Ocean
Xiaopu inter-arc ocean
Harlik arc
Dananhu arc
Central Tianshan arc
Kumishi ocean basin
Queershan arc
Mazongshan arc
Tarim block
Hongshishan inter-arc ocean
Huoshishan-Niujuanzi ophiolitic mélange
Huaniushan-Dundunshan arc
Dunhuang block
Liuyuan Ocean
Shibanshan arc
(c) Early Permian
Harlik arc
Central Tianshan arc
Bogda arc
Tu-Ha basin
Dananhu arc
Kumishi ocean
Queershan arc
Mazongshan arc
Tarim block
Hongshishan ophiolitic mélange
Hongyanjing inter-arc basin
Huoshishan-Niujuanzi ophiolitic mélange
Huaniushan-Dundunshan arc
Dunhuang block
Liuyuan Ocean
Shibanshan arc
Early Permian mafic–ultramafic Alaskan-type complexes (Ao et al., 2010)
(d) End Permian-Early Triassic
Harlik arc
Bogda arc
Tu-Ha basin
Dananhu arc
Kumishi ophiolite
Central Tianshan arc
southern Tianshan mélange
Queershan arc
Mazongshan arc
Tarim block
Hongshishan ophiolitic mélange
Hongyanjing inter-arc basin
Huoshishan-Niujuanzi ophiolitic mélange
Huaniushan-Dundunshan arc
Dunhuang block
Liuyuan ophiolitic mélange
Shibanshan arc
Cryptic suture: the thrust that separates the northerly accretionary units from the continental Tarim and Dunhuang blocks. Represents the termination of the consumed ocean (Xiao et al., 2013)

◂**Fig. 12** Schematic tectonic diagrams illustrating the evolution of the Beishan Orogenic Collage and the East Tianshan Orogenic Collage in the Paleozoic, where there are four phases of subductions and collisions: **a** in the Early Carboniferous, the Huaniushan–Dundunshan composite arc was accreted to the Mazongshan arc, which is correlated with the Harlik–Dananhu composite arc to the west. The Shibanshan formed in the northern margin of the Dunhuang Block, and the Central Tianshan arc formed by north-dipping subduction of the Tarim block; **b** Late Carboniferous extensional stage, when two arcs and one inter-arc basin formed because the composite arcs rifted: the Queershan arc formed to the north of the Hongshishan inter-arc basin in the BOC area, and the Harlik arc formed to the north of the Xiaopu inter-arc basin. Bimodal calc-alkaline volcanic rocks erupted in arc-related, subduction-related rifted arcs; **c** Early Permian. The Hongshishan Ocean and the Xiaopu Ocean closed, forming the Hongshishan ophiolitic mélange in the BOC and the Kelameili ophiolitic mélange in the Central Tianshan Orogenic Belt. In addition, the Hongyanjing inter-arc basin formed between the Huaniushan–Dundunshan arc and the Mazongshan in the BOC, while the Tu-Ha Basin formed between the Dananhu arc and the Bogda arc to the west; Notice that on the north margin of the Shibanshan arc, many ridge subduction-related Alaskan-type mafic–ultramafic complexes formed therein (Ao et al. 2010; Xiao et al. 2010); **d** in the End-Permian to Early Triassic, the Liuyuan Ocean closed in the BOC area forming the Liuyuan ophiolitic mélange, while the Kumishi Ocean (or South Tianshan Ocean) closed in the Central Tianshan Orogenic Belt forming the Kumishi ophiolite. A cryptic suture zone (modified after Xiao et al. 2013), which separates the upper plate (accretionary complex, fore-arc, and arc) from the lower plate with its passive margin and basement of the craton. All arcs, basins, ophiolitic mélanges, and accretionary wedges mutually amalgamated to form the East Tianshan Orogenic Collage and the Beishan Orogenic Collage, which belong to the southernmost central CAOB

120–180 km in Beishan–Gobi and southern Mongolia (Zheng et al. 1996).

Conclusions

The following conclusions can be drawn from our field and structural relations, and petrochemical and geochronological data of the Mazongshan arc and the Hongyanjing Basin.

1. The southern Mazongshan arc mainly consists of the Baishan Group that includes volcanic rocks and conglomerates, intruded by granodiorites. Permian to Triassic sediments were deposited in the northern margin of the Hongyanjing Basin and later strongly deformed. The boundary between the arc and the basin is the Pochengshan fault, which consists of ~1-km-wide mylonites and fault breccias.
2. The Mazongshan arc contains basaltic and pyroclastic rhyolite that have calc-alkaline geochemical signatures with an enrichment in large ion lithophile elements (LILE) such as Rb, Ba, and Pb, and a depletion in high field-strength elements (HFSE) (e.g., Nb and Ta). Also, the volcanic rocks show a slight enrichment in the LREE compared with the HREE. We conclude that these bimodal rocks were generated in an oceanic island arc and contaminated by fluids that were likely produced in a supra-subduction zone.
3. The granodiorite and pyroclastic rhyolite from the Mazongshan arc have zircon ages of 308.1 ± 3.8 Ma and 319.6 ± 3.4 Ma, respectively. Comparing the petrology, geochemistry, and age of the Mazongshan arc with equivalent data from the Bogda arc in the East Tianshan Orogenic Collage to the west, the Bogda arc is almost identical in all respects to the Mazongshan arc. We suggest that the bimodal calc-alkaline volcanic rocks in the Bogda and Mazongshan arcs were formed in a rifted subduction-generated arc, and not in post-orogenic rifts affected by mantle plumes. We therefore conclude that the volcanic rocks were extruded in inter-arc, intra-arc or back-arc basins or rifting margins.
4. Combining with data from our previous studies in the BOC and East Tianshan Orogenic Collage, we present a new model for their tectonic evolution from the Early Carboniferous to the Early Permian–Early Triassic, which better illustrates the evolution of different terranes and their accretionary and collisional events. The final suture zone in the BOC and East Tianshan Orogenic Collage is cryptic. It separates the upper plate units (accretionary complex, fore-arc and arc) from the lower plate units (passive margin and cratonic basement).

Acknowledgements We thank Dick Glen, Shoufa Lin, Nathan Cleven, Bo Wan, and Songjian Ao for their helpful discussions and assistance in joint field trips. Constructive comments and suggestions from Journal reviewers, Timothy Kusky and John Wakabayashi, are greatly appreciated. This work was financially supported by the 973 Program (2014CB440801), the Strategic Priority Research Program (B) of the Chinese Academy of Sciences (XDB18020203), the Key Research Program of Frontier Sciences, CAS (QYZDJ-SSW-SYS012), National Natural Science Foundation of China (41402183, 41230207, 41390441, and 41190075), and State Key Laboratory of Earthquake Dynamics (LED2013B03). This is a contribution to IGCP 592.

Appendix: Analytical methods

Major and trace elements

Fresh igneous rocks (including the intrusive rocks 11pcs13-2, 11pcs13-3, and 11pcs14-2, and the extrusive rocks 11pcs15-2, 11pcs18-3, 11pcs18-4, 11pcs20-1, 11pcs21-2, 11pcs23-2, 11pcs24-2, and 11pcs24-3) were selected for major and trace element analysis in the Institute of Geology and Geophysics, Chinese Academy of Sciences (IGGCAS) in Beijing.

For major element analyses, mixtures of whole-rock powder (0.5 g) and $Li_2B_4O_7$ + $LiBO_2$ (5 g) were heated

and fused into glass disks and analyzed by X-ray fluorescence spectroscopy (XRF) with an AXIOS Minerals spectrometer. The analytical uncertainties were generally within 0.1–1% (RSD). Loss on ignition (LOI) was obtained using 0.5 g powder heated to 1100 °C for 1 h. For trace element analyses, whole-rock powders (40 mg) were dissolved in distilled HF + HNO_3 in Teflon screw-cap capsules at 200 °C for 5 days, dried, and then digested with HNO_3 at 150 °C for 1 day, and the final step was repeated. Dissolved samples were diluted to 49 ml with 1% HNO_3, and 1 ml 500 ppb indium was added to the solution as an internal standard (In). Trace elements and REE abundances were determined by inductively coupled plasma mass spectrometry (ICP–MS) using a Finnigan MAT ELEMENTI spectrometer, which has analytical uncertainties within 5% for most elements. All the major and trace element analyses are listed in Supplementary Table 1.

Zircon cathodoluminescence and geochronology

Two igneous rocks, 11pcs18 and 11pcs13 from the Mazongshan arc (Fig. 3), were selected for zircon U–Pb dating. After sample crushing, >100 zircon grains were sorted by standard heavy liquid and magnetic techniques. Representative zircons were selected and mounted on adhesive tape, then enclosed in epoxy resin, and polished. CL images were made using a SX51 Electron Probe Microanalyzer for high-resolution imaging and spectroscopy at the IGGCAS. The acceleration voltage during the CL imaging was 15 kV.

For all the samples, isotopic measurements were taken using an Agilent 7500a quadrupole (Q)-ICPMS at the LA–MC–ICPMS laboratory of the IGGCAS in Beijing. $^{207}Pb/^{206}Pb$ and $^{206}Pb/^{238}U$ ratios were calculated using GLITTER 4.0 (Griffin et al. 2008). Standards were one zircon 91500 and one Gj-1. The relative standard deviations of reference values for 91500 were set at 2%. Detailed analytical procedures and experimental parameters are listed in Xie et al. (2008). The age data are shown in Supplementary Tables 2 and 3.

References

Allen MB, Windley BF, Zhang C (1994) Cenozoic tectonics in the Urumgi-Korla region of the Chinese Tien Shan. Geol Rundsch 83:406–416

Ao SJ, Xiao WJ, Han CM, Mao QG, Zhang JE (2010) Geochronology and geochemistry of Early Permian mafic–ultramafic complexes in the Beishan area, Xinjiang, NW China: implications for late Paleozoic tectonic evolution of the southern Altaids. Gondwana Res 18:466–478

Ao SJ, Xiao WJ, Han CM, Li XH, Qu JF, Zhang JE, Guo QQ, Tian ZH (2012) Cambrian to early Silurian ophiolite and accretionary processes in the Beishan collage, NW China: implications for the architecture of the Southern Altaids. Geol Mag 149:606–625

Ao SJ, Xiao WJ, Windley BF, Mao QG, Han CM, Zhang JE, Yang L, Geng JZ (2016) Paleozoic accretionary orogenesis in the eastern Beishan orogen: constraints from zircon U–Pb and $^{40}Ar/^{39}Ar$ geochronology. Gondwana Res 30:224–235

Boersma M, Broekmeyer LM (1987) Index of figured plant megafossils Permian 1976–1980. Rev Palaeobot Palynol 53:11–139

Buslov MM, Watanabe T, Fujiwara Y, Iwata K, Saphonova YI, Obut OT, Sugai Y (2001) Geodynamics and tectonics of Central Asia: continental growth in Vendian-Paleozoic time. Gondwana Res 4:587

Carroll AR, Graham SA, Hendrix MS, Ying D, Zhou D (1995) Late Paleozoic tectonic amalgamation of northwestern China: sedimentary record of the northern Tarim, northwestern Turpan, and southern Junggar Basins. Geol Soc Am Bull 107:571–594

Cawood PA, Kröner A, Collins WJ, Kusky TM, Mooney WD, Windley BF (2009) Accretionary orogens through Earth history. Geol Soc Lond Spec Publ 318:1–36

Chen XJ, Shu LL, Santosh M (2011) Late Paleozoic post-collisional magmatism in the Eastern Tianshan Belt, Northwest China: new insights from geochemistry, geochronology and petrology of bimodal volcanic rocks. Lithos 127:581–598

Chen XJ, Shu LL, Santosh M, Zhao XX (2013) Island arc-type bimodal magmatism in the eastern Tianshan Belt, Northwest China: geochemistry, zircon U–Pb geochronology and implications for the Paleozoic crustal evolution in Central Asia. Lithos 168–169:48–66

Dai WJ, Gong QS (2000) Redividing the"Lebaquan Group" in Beishan area of Gansu Province and its geological implication. Acta Geol Gansu 9:23–29 **(in Chinese with English abstract)**

Davis GA, Zheng Y, Wang C, Darby BJ, Zhang C, Gehrels GE (2001) Mesozoic tectonic evolution of the Yanshan fold and thrust belt, with emphasis on Hebei and Liaoning provinces, northern China. In: Hendrix MS, Davis GA (eds) Paleozoic and mesozoic tectonic evolution of Central and Eastern Asia: from continental assembly to intracontinental deformation, vol 194. Geological Society of America Memoir, Boulder, Colorado, pp 171–197

Du G, Li WH, Yang WB, Wang W, Bai YL (2003) The main characteristics of Lebaquan-Gongpoquan epicontinental arc and the dynamic background for its forming in the contiguous area across Gansu, Xinjiang and Inner Mongolia. Acta Geol Gansu 12:16–20 **(in Chinese with English abstract)**

GBGMR (1969) The geological report of Niujuanzi Map. The second survey team of regional geology. Gansu Bureau of Geology and Mineral Resources, Changye Five-Four-Three Publishing House, scale 1:200,000

GBGMR (2001) The geological report of Mazongshan Map. No.3 Geological Survey Team of the Gansu Bureau of Geology and Mineral Deposits scale 1:250,000

Gong QS, Liu MQ, Li HL, Liang MH, Dai WJ (2003) The type and basic characteristics of Beishan orogenic belt, Gansu. Northwest Geol 35:28–34 **(in Chinese with English abstract)**

Griffin W, Powell W, Pearson N, O'Reilly S (2008) GLITTER: data reduction software for laser ablation ICP-MS. Laser Ablation-ICP-MS in the Earth Sciences Short Course Series 40. Mineralogical Association of Canada, pp 204–207

Guo QQ, Xiao WJ, Windley BF, Mao QG, Han CM, Qu JF, Ao SJ, Li JL, Song DF, Yong Y (2012) Provenance and tectonic settings of Permian turbidites from the Beishan Mountains, NW China: implications for the Late Paleozoic accretionary tectonics of the southern Altaids. J Asian Earth Sci 49:54–68

Guo QQ, Xiao WJ, Hou QL, Windley BF, Han CM, Tian ZH, Song DF (2014) Construction of Late Devonian Dundunshan arc in the Beishan orogen and its implication for tectonics of southern Central Asian Orogenic Belt. Lithos 184–187:361–378

He SP, Ren BS, Yao WG, Fu LP (2002) The division of tectonic units of Beishan area, Gansu-Inner Mongolia. Northwest Geol 35:29–40 **(in Chinese with English abstract)**

Hendrix MS, Beck MA, Badarch G, Graham SA (2001) Triassic synorogenic sedimentation in southern Mongolia: Early effects of intracontinental deformation. In: Hendrix MS, Davis GA (eds) Paleozoic and Mesozoic tectonic evolution of Central and Eastern Asia: from continental assembly to intracontinental deformation, vol 194. Geological Society of America Memoir, Boulder, Colorado, pp 389–412

Huang ZB, Jin X (2006) Geological characteristics and its setting for volcanic rocks of Baishan formation in Hongshishan area of Gansu Province. Gansu Geol 15:19–24 **(in Chinese with English abstract)**

Jahn BM (2004) The Central Asian Orogenic Belt and growth of the continental crust in the Phanerozoic. Geol Soc Lond Spec Publ 226:73–100

Johnson CL, Webb LE, Graham SA, Hendrix MS, Badarch G (2001) Sedimentary and structural records of late Mesozoic high-strain extension and strain partitioning, East Gobi basin, southern Mongolia. In: Hendrix MS, Davis GA (eds) Paleozoic and mesozoic tectonic evolution of Central and Eastern Asia: from continental assembly to intracontinental deformation, vol 194. Geological Society of America Memoir, pp 413–434

Lamb MA, Badarch G, Navratil T, Poier R (2008) Structural and geochronologic data from the Shin Jinst area, eastern Gobi Altai, Mongolia: implications for Phanerozoic intracontinental deformation in Asia. Tectonophysics 451:312–330

Liu XY, Wang Q (1995) Tectonics and evolution of the Beishan orogenic belt, West China. Geol Res 10:151–165

Ma XX, Shu LS, Santosh M, Li JY (2012) Detrital zircon U–Pb geochronology and Hf isotope data from Central Tianshan suggesting a link with the Tarim Block: implications on Proterozoic supercontinent history. Precambr Res 206–207:1–16

Mao QG, Xiao WJ, Windley BF, Han CM, Qu JF, Ao SJ, Zhang JE, Guo QQ (2012) The Liuyuan complex in the Beishan, NW China: a Carboniferous-Permian ophiolitic fore-arc sliver in the southern Altaids. Geol Mag 149:483–506

Mao QG, Xiao WJ, Fang TH, Windley BF, Sun M, Ao SJ, Zhang JE, Huang XK (2014) Geochronology, geochemistry and petrogenesis of Early Permian alkaline magmatism in the Eastern Tianshan: implications for tectonics of the Southern Altaids. Lithos 190–191:37–51

Nie FJ, Jiang SH, Bai DM, Wang XL, Su XX, Li JC, Liu Y, Zhao XM (2002) Metallogenic studies and ore prospecting in the conjunction area of Inner Mongolia Autonomous Region, Gansu Province and Xinjiang Uygur Autonomous Region (Beishan Mt), northwest China, Beijing. Geological Publishing House, Beijing (**in Chinese with English abstract**)

Pearce JA (1982) Trace element characteristics of lavas from destructive plate boundaries. In: Thorpe RS (ed) Andesites. Wiley, New York, pp 525–548

Pearce JA (1996) A user's guide to basalt discrimination diagrams In: Wyman DA (ed) Trace element geochemistry of volcanic rocks. Applications for massive sulphide exploration. Geological Association of Canada 12, Short Course Notes: pp 79–113

Peceerillo R, Taylor SR (1976) Geochemistry of Eocene calc-alkaline volcanic rocks from the Kastamonu area northern Turkey. Contrib Miner Petrol 58:63–81

Rudnick RL, Gao S (2003) Vol 3: the crust, 301—the composition of the continental crust. In: Holland HD, Turekian KK (eds) Treatise on geochemistry. Elsevier-Pergamon, Oxford, pp 1–64

Sengör AC, Natal'In BA (1996) Turkic-type orogen and its role in the making of the continental crust. Annu Rev Earth Planet Sci 24:263–337

Sengör A, Natalin BA, Burtman V (1993) Evolution of the Altaid tectonic collage and Palaeozoic crustal growth in Eurasia. Nature 364:299–307

Sheth HC, Torres-Alvarado IS, Verma SP (2002) What is the "Calc-alkaline Rock Series"? Int Geol Rev 44:686–701

Shu LL, Wang B, Zhu WB, Guo ZJ, Charvet J, Zhang Y (2011) Timing of initiation of extension in the Tianshan, based on structural, geochemical and geochronological analyses of bimodal volcanism and olistostrome in the Bogda Shan (NW China). Int J Earth Sci 100:1647–1663

Song DF, Xiao WJ, Han CM, Tian ZH (2013) Geochronological and geochemical study of gneiss–schist complexes and associated granitoids, Beishan Orogen, southern Altaids. Int Geol Rev 55:1705–1727

Su BX, Qin K-Z, Sakyi PA, Liu P-P, Tang D-M, Malaviarachchi SPK, Xiao Q-H, Sun H, Dai Y-C, Yan H (2011) Geochemistry and geochronology of acidic rocks in the Beishan region, NW China: petrogenesis and tectonic implications. J Asian Earth Sci 41:31–43

Sun SS, McDonough WF (1989) Chemical and isotopic systematics of oceanic basalts: implications for mantle composition and processes. Geol Soc Lond Spec Publ 42:313–345

Tian ZH, Xiao WJ, Shan YH, Windley BF, Han CM, Zhang JE, Song DF (2013) Mega-fold interference patterns in the Beishan orogen (NW China) created by change in plate configuration during Permo-Triassic termination of the Altaids. J Struct Geol 52:119–135

Tian ZH, Xiao WJ, Windley BF, Lin LN, Han CM, Zhang JE, Wan B, Ao SJ, Song DF, Feng JX (2014) Structure, age, and tectonic development of the Huoshishan-Niujuanzi ophiolitic mélange, Beishan, southernmost Altaids. Gondwana Res 25:820–841

Tian ZH, Xiao WJ, Sun JM, Windley BF, Glen R, Han CM, Zhang ZY, Zhang JE, Wan B, Ao SJ, Song DF (2015) Triassic deformation of Permian Early Triassic arc-related sediments in the Beishan (NW China): last pulse of the accretionary orogenesis in the southernmost Altaids. Tectonophysics 662:363–384

Tian ZH, Xiao WJ, Zhang ZY, Lin X (2016) Fisson-track constrains on superposed folding in the Beishan orogenic belt, southernmost Altaids. Geosci Front 7:181–196

Wang F, Wei Z, Zhang G, Sun X (2004) New data of Silurian strata in areas of Hongshishan, North Beishan Mountains, Gansu Province of China. Geol Bull China 23:1162–1163 **(in Chinese with English abstract)**

Wang JR, Li TD, Tian LP, Yu M, Wang HT, Zhao ZX, Tang ZL (2010a) LatePaleozoic tectonic-magmatic evolution in Bogda Orogenic belt, Xinjiang: evidence from geochemistry of volcanic rocks. Acta Petrol Sin 26:1103–1115 **(in Chinese with English abstract)**

Wang Y, Sun GH, Li JY (2010b) U–Pb (SHRIMP) and 40Ar/39Ar geochronological constraints on the evolution of the Xingxingxia shear zone, NW China: a Triassic segment of the Altyn Tagh fault system. Geol Soc Am Bull 122:487–505

Webb LE, Johnson CL (2006) Tertiary strike-slip faulting in southeastern Mongolia and implications for Asian tectonics. Earth Planet Sci Lett 241:323–335

Wei ZJ, Huang ZB, Sun J, Huo JC (2004) Geological characteristics of ophiolite migmatitic complex of Hongshishan region, Gansu. Northwest Geol 37:13–18 **(in Chinese with English abstract)**

Wilhem C, Windley BF, Stampfli GM (2012) The Altaids of Central Asia: a tectonic and evolutionary innovative review. Earth Sci Rev 113:303–341

Windley BF, Alexeiev D, Xiao WJ, Kröner A, Badarch G (2007) Tectonic models for accretion of the Central Asian Orogenic Belt. J Geol Soc 164:31–47

Xia LQ, Xia ZC, Xu XY, Li XM, Ma ZP (2008) Relative contributions of crust and mantle to the generation of the Tianshan Carboniferous rift-related basic lavas, northwestern China. J Asian Earth Sci 31:357–378

Xiao WJ, Windley BF, Hao J, Zhai MG (2003) Accretion leading to collision and the Permian Solonker suture, Inner Mongolia, China: termination of the central Asian orogenic belt. Tectonics 22(6):1069. doi:10.1029/2002TC001484

Xiao WJ, Zhang LC, Qin KZ, Sun S, Li JL (2004) Paleozoic accretionary and collisional tectonics of the Eastern Tianshan (China): implications for the continental growth of Central Asia. Am J Sci 304:370–395

Xiao WJ, Windley BF, Yuan C, Sun M, Han CM, Lin SF, Chen HL, Yan QR, Liu DY, Qin KZ, Li JL, Sun S (2009) Paleozoic multple subduction-accretion processes of the southern Altaids. Am J Sci 309:221–270

Xiao WJ, Mao QG, Windley BF, Han CM, Qu JF, Zhang JE, Ao SJ, Guo QQ, Cleven NR, Lin SF, Shan YH, Li JL (2010) Paleozoic multiple accretionary and collisional processes of the Beishan orogenic collage. Am J Sci 310:1553–1594

Xiao WJ, Windley BF, Allen MB, Han C (2013) Paleozoic multiple accretionary and collisional tectonics of the Chinese Tianshan orogenic collage. Gondwana Res 23:1316–1341

Xiao WJ, Windley BF, Sun S, Li JL, Huang BC, Han CM, Yuan C, Sun M, Chen H (2015) A tale of amalgamation of three Permo-Triassic Collage Systems in Central Asia: oroclines, sutures, and terminal accretion. Annu Rev Earth Planet Sci 43:477–507. doi:10.1146/annurev-earth-060614-105254

Xie LW, Zhang Y, Zhang HH, Sun J, Wu FY (2008) In situ simultaneous determination of trace elements, U–Pb and Lu–Hf isotopes in zircon and baddeleyite. Chin Sci Bull 53:1565–1573

Xie W, Song XY, Deng YF, Wang YS, Ba DH, Zheng WQ, Li XB (2012) Geochemistry and petrogenetic implications of a Late Devonian mafic–ultramafic intrusion at the southern margin of the Central Asian Orogenic Belt. Lithos 144–145:209–230

Xu XY, He SP, Wang HL, Chen JL, Zhang EP, Feng YM (2008) Outline of the Geology of NW China—Qinling, Qilian and Tian Shan Areas. Science in China Press, Beijing **(in Chinese with English abstract)**

Zhang J, Cunningham D (2012) Kilometer-scale refolded folds caused by strike-slip reversal and intraplate shortening in the Beishan region, China. Tectonics 31:TC3009

Zhang ZY, Zhu WB, Zheng DW, Zheng BH, Yang WM (2016) Apatite fission track thermochronology in the Kuluketage and Aksu areas, NW China: implication for tectonic evolution of the northern Tarim. Geosci Front 7:171–180

Zheng YD, Zhang Q, Wang Y, Liu R, Wang SG, Zuo G, Wang SZ, Lkaasuren B, Badarch G, Badamgarav Z (1996) Great Jurassic thrust sheets in Beishan (North Mountains)—Gobi areas of China and southern Mongolia. J Struct Geol 18:1111–1126

Zhou H, Chen L, Sun Y, Zhu T (2016) Tectonic framework of Late Paleozoic intrusions in Xingxingxia: implications for final closure of South Tianshan Ocean in East Tianshan. Acta Geol Sin (Engl Edit) 90:801–824

Zuo GC, Zhang SL, He GQ, Zhang Y (1990a) Early Paleozoic plate tectonics in Beishan area. Sci Geol Sin 4:305–314

Zuo GC, Zhang SL, Wang X, Jin SQ, He GQ, Zhang Y, Li HC, Bai WC (1990b) Plate tectonics and metallogenic regularities in Beishan Region. Peking University Publishing House, Beijing, 48 pp (**in Chinese with English abstract**)

Zuo GC, Zhang S, He G, Zhang Y (1991) Plate tectonic characteristics during the early Paleozoic in Beishan near the Sino-Mongolian border region, China. Tectonophysics 188:385–392